HHS Public Access

Author manuscript

Cell Rep. Author manuscript; available in PMC 2024 December 08.

Published in final edited form as:

Cell Rep. 2024 November 26; 43(11): 114877. doi:10.1016/j.celrep.2024.114877.

Activity-assembled nBAF complex mediates rapid immediate early gene transcription by regulating RNA polymerase II productive elongation

Karen G. Cornejo[1], **Andie Venegas**[1], **Morgan H. Sono**[1], **Madeline Door**[1], **Brenda Gutierrez-Ruiz**[1], **Lucy B. Karabedian**[1], **Supratik G. Nandi**[1], **Marco Hadisurya**[2], **W. Andy Tao**[2,3], **Emily C. Dykhuizen**[3], **Ramendra N. Saha**[1,4,*]

[1]Molecular and Cell Biology Department, School of Natural Sciences, University of California, Merced, 5200 North Lake Road, Merced, CA 95343, USA

[2]Department of Biochemistry, Purdue University, West Lafayette, IN 47907, USA

[3]Purdue University Institute for Cancer Research, Department of Medicinal Chemistry and Molecular Pharmacology, Purdue University, West Lafayette, IN 47907, USA

[4]Lead contact

SUMMARY

Signal-dependent RNA polymerase II (RNA Pol II) productive elongation is an integral component of gene transcription, including that of immediate early genes (IEGs) induced by neuronal activity. However, it remains unclear how productively elongating RNA Pol II overcomes nucleosomal barriers. Using RNAi, three degraders, and several small-molecule inhibitors, we show that the mammalian switch/sucrose non-fermentable (SWI/SNF) complex of neurons (neuronal BRG1/BRM-associated factor or nBAF) is required for activity-induced transcription of neuronal IEGs, including Arc. The nBAF complex facilitates promoter-proximal RNA Pol II pausing and signal-dependent RNA Pol II recruitment (loading) and, importantly, mediates productive elongation in the gene body via interaction with the elongation complex and elongation-competent RNA Pol II. Mechanistically, RNA Pol II elongation is mediated by activity-induced nBAF assembly (especially ARID1A recruitment) and its ATPase activity. Together, our data demonstrate that the nBAF complex regulates several aspects of RNA Pol II transcription and reveal mechanisms underlying activity-induced RNA Pol II elongation. These findings may

*Correspondence: rsaha3@ucmerced.edu.

AUTHOR CONTRIBUTIONS

K.G.C., A.V., and M.H.S. performed experiments, curated and validated data, performed formal analyses, and edited the manuscript. K.G.C. co-wrote the first draft. M.D., B.G.-R., L.B.K., S.G.N., and M.H. performed experiments and acquired data. E.C.D. and W.A.T. provided expertise and feedback. E.C.D. additionally provided reagents. R.N.S. conceptualized, supervised, and administered the project; performed experiments; visualized figures; and wrote the first draft. The manuscript was revised by R.N.S. and K.G.C. R.N.S. and E.C.D. acquired funding. All authors reviewed the manuscript.

DECLARATION OF INTERESTS

The authors declare no competing interests.

SUPPLEMENTAL INFORMATION

Supplemental information can be found online at https://doi.org/10.1016/j.celrep.2024.114877.

offer insights into human maladies etiologically associated with mutational interdiction of BAF functions.

Graphical Abstract

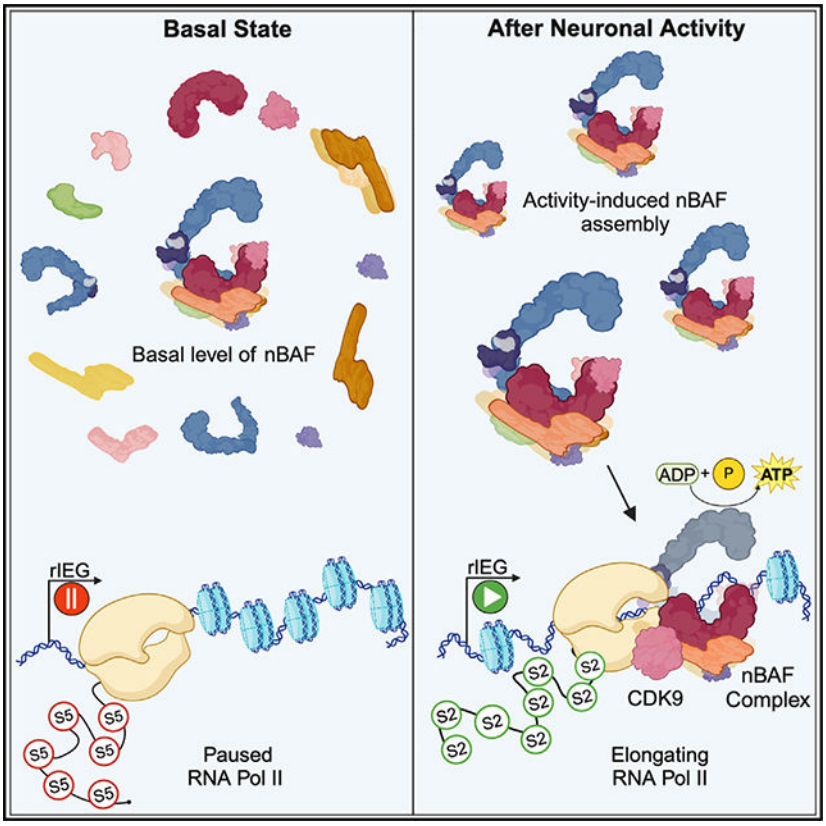

In brief

Cornejo et al. demonstrate that the neuronal BAF chromatin remodeling complex is necessary for productive elongation of RNA Pol II and activity-induced gene transcription. Such regulatory role is mediated mechanistically by activity-induced nBAF assembly and its ATPase activity.

INTRODUCTION

BRG1/BRM-associated factor (BAF) complexes are conserved ATP-dependent chromatin remodelers. They were first discovered in yeast as the SWI/SNF (switch/sucrose non-fermentable) complex,[1–3] then in *Drosophila*,[4] and in mammals soon after.[5,6] Mammalian BAF complexes are now known to be multimeric large complexes weighing 1–2 MDa, which are formed combinatorially with products of 31 genes. Three biochemically distinct BAF complexes are delineated in mammals: canonical BAF (cBAF), polybromo-associated BAF (PBAF), and GLTSCR1-BAF (GBAF),[7] also called non-canonical BAF (ncBAF)[8] (Figure 1A). All three complexes feature either SMARCA4 (BRG1) or SMARCA2 (BRM) as the ATPase core unit, which interacts with several other subunits to form functional complexes. The quintessential cBAF complex utilizes 12–15 subunits, including SMARCC1

(BAF155) and/or SMARCC2 (BAF170) as scaffolding subunits[9–12] and ARID1A or ARID1B as mutually exclusive sub-complex-defining subunits. Combinatorial assemblies around these core components in a modular fashion permute several functional BAF complexes.[13,14]

BAF complexes drive transcriptional programs, such as those mediating differentiation and lineage specification of developing cells.[15] Developmental programs often include compositional transformations of cBAF complexes. For example, during neuro-genesis, the neuronal progenitor version of the cBAF complex (npBAF), which features SS18, DPF2, and ACTL6A (BAF53a), swaps several subunits to become the neuronal BAF (nBAF) complex, which is instead characterized by SS18L1 (CREST), DPF1/3, and ACTL6B (BAF53b).[10] The transition from npBAF to nBAF also includes shifts in subunit stoichiometry, such as increasing SMARCC2 ratios compared to SMARCC1. The nBAF is both “necessary” and “sufficient” for neurogenesis. Forcing nBAF expression in human fibroblasts converts them to neurons,[16,17] while knocking out nBAF subunits in developing neurons causes defective synaptogenesis.[18,19] Moreover, mutations in genes encoding several BAF subunits disrupt neurodevelopment[10,12,20–22] and coincide with human neurodevelopmental disorders (NDDs), including intellectual disability (ID) and autism spectrum disorders (ASDs).[20,23–27] Genes encoding the cBAF subunit possess the greatest number of *de novo* missense and protein-truncating mutations among all nuclear protein complexes.[28] Together, it is clear that nBAF drives neuron-specific gene transcription in developing and mature neurons,[19,29] and NDDs may result from loss of such function. However, the underlying molecular mechanisms thereof are understood vaguely.

BAF complexes are primarily alluded to as chromatin remodelers, which refers to their ability to reposition, evict, or disassemble nucleosomes. Related to this core function, BAF complexes also play several roles in gene transcription. In yeast, the SWI/SNF complex actively decondenses chromatin, antagonizes chromatin-mediated transcriptional repression, and acts as a gene transcription activator.[30,31] In mammals, BAF complexes work in concert with many transcription factors to promote chromatin accessibility and transcription.[32] They are enriched at promoters and enhancers, where these complexes are implicated in promoter-enhancer interactions, enhancer maintenance, and activation of lineage-specific enhancers.[33–36] Recently, they were correlated with promoter-proximal RNA polymerase II (RNA Pol II) pausing[37] and shown to be necessary for activation of inducible promoters.[38] However, it remains unclear if BAF complexes are necessary for RNA Pol II productive elongation.

Productive elongation requires a signal-directed switch of RNA Pol II from its obligatory promoter-proximal paused state to active transcription. This process is orchestrated by positive transcription elongation factor b (P-TEFb), the master regulator of transcription elongation.[39] CDK9, the constituent kinase in P-TEFb, phosphorylates the second serine (S2) in C-terminal domain (CTD) heptad repeats of Rpb1, the largest RNA Pol II subunit. The phosphorylated CTD acts as a scaffold for elongation factors such as SPT6, which assemble to form the elongation complex (EC).[40,41] The EC increases elongation competency and drives RNA Pol II several-fold faster than isolated RNA Pol II.[42] Notwithstanding such insights, however, it remains unclear how RNA Pol II

overcomes nucleosomes in the gene body during productive elongation. Elongating RNA Pol II complexes can surmount nucleosomal barriers without needing remodelers,[43] but inefficiently. Therefore, one presumes that efficient elongation is aided by nucleosome remodelers. However, the relationship between the EC and any such remodeler remains unclear.

Indirect evidence in the literature suggests that the BAF complex may have a role during RNA Pol II elongation. SWI/SNF components were reported in transcribing gene bodies of yeast and *Drosophila*.[44–49] Brm immunostaining in *Drosophila* polytene chromatin localizes to active chromatin, and depletion of Brm reduces global transcription.[46] In yeast, Swi2 and RNA Pol II occupancy was identical in the coding region of an osmotically induced gene.[44] SMARCA2 and SMARCA4 are found in the coding region of several genes, where they aid in alternative splicing.[47] Finally, in a cellular artificial construct, Brg1 facilitated nucleosome traversal by RNA Pol II.[45] Taken together, these results indicate the association of the BAF complex with RNA Pol II elongation, but the underlying mechanisms thereof remain obscure, especially in mammalian systems.

To investigate any role of nBAF in RNA Pol II elongation, we focused on neuronal activity-induced gene transcription. We have shown previously that in response to membrane activity, neurons undertake a gene transcription program whereby three distinct classes of genes are briskly expressed in temporally distinct waves: rapid immediate early genes (rIEGs), delayed immediate early genes (dIEGs), and secondary genes that require *de novo* protein translation.[50] The earliest among them are rIEGs, a small subset of 15–18 genes (e.g., *Arc*) whose transcription happens when few or no other genes undergo inducible transcription. Promoters of rIEGs have open chromatin and are preloaded with necessary transcription factors and paused RNA Pol II nearby.[50,51] Upon stimulation, the pioneer RNA Pol II undertakes productive elongation and pre-mRNA production within minutes. Additional rounds of RNA Pol II recruitment enable a robust transcriptional response. This process requires the fast-acting MAP kinase pathway,[50] which regulates several transcription factors and also the pTEFb.[52] Using *Arc* and other rIEGs as model genes, we demonstrate in dissociated primary rat neurons that nBAF mediates activity-induced rapid transcription. We also show that the nBAF complex assembles in response to activity, interacts as a key component with the EC, and utilizes ATPase activity to facilitate RNA Pol II elongation.

RESULTS

BAF complex and its ATPase activity are necessary for activity-induced rIEG transcription

Does neuronal-activity-induced rapid gene transcription require the BAF complex? To answer, we utilized several pharmacological inhibitors, degraders, and RNAi. First, we used the recently developed ACBI1, the proteolysis-targeting chimera (PROTAC) degrader of BAF ATPases (SMARCA2 and SMARCA4) and associated subunits.[53] Dissociated rat cortical neurons were treated with ACBI1 for 3 h, and several nBAF subunit levels were estimated. ACBI1, but not its negative control (inactive *cis*-ACBI1), reduced DPF1, ACTL6B, and SMARCA4 to beneath detection levels (Figures 1B and 1C). Levels of SMARCC2, ARID1A, ARID1B, and SS18L1 were reduced but not eliminated (Figures 1B, 1D, and 1E). Therefore, ACBI1 degrades major BAF complex subunits to various degrees

but leaves intact some protein orphans from the complex, such as SMARCC2 and SS18L1. Next, sustained synaptic activity was stimulated with bicuculline and 4-aminopyridine (Bic + 4AP) for 15 min, and transcriptional response was assessed by quantifying *Arc* pre-mRNA.[54,55] Fifteen minutes of activity was chosen to isolate transcription of rIEGs from other activity-induced transcription, which is detectable later in the hour.[50,51] ACBI1, but not *cis*-ACBI1, significantly attenuated activity-induced *Arc* transcription (Figure 1F). To rule out an *Arc*-specific effect, eight other rIEGs were additionally tested. All eight rIEGs displayed sensitivity to ACBI1, but not to *cis*-ACBI1 (Figure S1A), suggesting a general role of the complex in activity-induced rIEG transcription. Furthermore, significant transcriptional impairment also resulted when neurons were preincubated with two small-molecule allosteric BAF ATPase inhibitors, BRM014 and FHT1015[56,57] (Figure 1G). Together, the combined use of pharmacological degradation and inhibition of the BAF complex ATPase function suggests that BAF plays a key role in activity-induced transcription of *Arc* and other rIEGs.

To further validate the involvement of the BAF complex in activity-induced transcription of IEGs, we knocked down two BAF complex subunits via short hairpin RNA. Dissociated cortical neurons were infected with RNAi targeting SMARCC2[58] or ARID1A, the scaffolding and nBAF-defining subunits, respectively. Protein levels of both targeted proteins were reduced, confirming RNAi efficacy (Figures 2A and 2B). Consistent with the above assays involving the degrader and ATPase inhibitors, SMARCC2 and ARID1A knockdown significantly impaired *Arc* transcription following Bic treatments (Figure 2C). Together, these data portray the BAF complex as a positive regulator of activity-induced transcription. Also, transcriptional impairment due to ARID1A depletion suggests involvement of the nBAF complex in the process.

Activity-assembled nBAF complex drives rIEG transcription

Several recently described nBAF-, PBAF-, and GBAF-specific inhibitors were used next to characterize the BAF complex regulation of rIEG transcription. First, we used BD98, a recently described cBAF inhibitor that specifically inhibits ARID1A-containing complexes.[59] To validate direct binding of BD98 with the nBAF complex, we performed cellular thermal shift assay (CETSA[60]), which reports thermal stabilization of proteins upon ligand binding in cells. Treating neurons with BD98 enhanced the thermal stability of SMARCC2, SMARCA4, and nBAF-specific DPF1 (Figure 2D), suggesting direct binding of BD98 with the nBAF complex. CETSA could not be performed with ARID1A due to its low abundance. Instead, we performed coimmunoprecipitation assays of endogenous proteins (henceforth, coIP) in the presence of BD98. The inhibitor was expected to disrupt nBAF subunit interactions, especially those of ARID1A. Here, we made an unexpected discovery. Compared to the untreated control, interactions of SMARCC2 with ARID1A, SMARCA4, and SS18L1 increased after Bic + 4AP treatment (Figure 2E), suggesting an activity-induced assembly of the nBAF complex (Figure 2E and S2). This assembly—especially recruitment of ARID1A— was inhibited by BD98 (Figures 2E and S2).

Next, the effect of BD98 on rIEG transcription was assessed along with PBAF- and GBAF-specific inhibitors (2–77[61] and I-BRD9,[62] respectively). Pretreatment with BD98,

but not PBAF or GBAF inhibitor, significantly attenuated activity-induced transcription of *Arc* and other rIEGs (Figure 2F and S1A). Furthermore, we also used VZ185, the BRD7 and BRD9 PROTAC degrader.[63] Three hours of treatment with VZ185 depleted BRD7, but not the nBAF subunit DPF1 or the core subunit SMARCC2 (Figure S1B). We did not detect BRD9 in neuronal extracts with two commercially available antibodies. Like PBAF and GBAF inhibitors, and in contrast to BD98, VZ185 did not affect activity-induced *Arc* induction (Figure 2F). BD98 acted in a dose-dependent manner, whereby 5 μM significantly inhibited *Arc* transcription (Figure 2G) and was therefore used as the effective dose for all other assays. Toward due diligence, we checked for any non-specific upstream effects of BD98 by testing its impact on activity-induced MAP kinase activation, a key signaling pathway for rIEGs,[50] and found none at 5 μM or less concentration (Figure S1C). Similarly, ACBI-mediated degradation of BAF subunits did not influence activity-induced MAP kinase activation (Figure S1D).

To further corroborate signal-induced nBAF complex assembly, additional assays were performed. First, we tested for involvement of long nucleic acids in complex assembly by nuclease digestion of DNA and RNA during coIP. Such digestion did not alter induced SMARCC2-ARID1A interactions (Figures S3A and S3B), suggesting that the complex assembly is not dependent on long stretches of nucleic acids (but may be facilitated by shorter protected ones[64]). Second, we extracted nuclear content using high salt and verified activity-induced enhanced SMARCC2-ARID1A (as a stand-in for complex assembly) interactions in this chromatin-free nuclear extract[65] (Figures S3C and S3D). Third, to define components of the assembled complex, we performed SMARCC2 immunoprecipitation with quantitative mass spectrometry-based proteomic analysis of eluted proteins (IP-MS). Our IP-MS studies showed significant activity-induced upregulation of SMARCC2 interactions with several nBAF subunits (Figure 3A), but not with members of PBAF or GBAF. Last, we assayed for the assembled complex under more stringent conditions. Modifying a published cell fractionation protocol[66,67] for non-dividing neurons, we purified neuronal chromatin fraction using high salt (300 mM NaCl) and 1 M urea (Figure 3B). The chromatin fraction was verified by elongation-competent RNA Pol II (Rpb1-pS2). SMARCC2 coIP was performed with this fraction. Enhanced SMARCC2-ARID1A interactions were observed in the chromatin fraction in response to activity. Such interactions were significantly sensitive to BD98 (Figures 3C and 3D). Furthermore, we extracted RNA from the chromatin fraction and assayed for nascent transcripts. Mirroring data displayed in Figures 1F, 2C, and S1A, depleting or inhibiting the BAF complex with ACBI or BD98, respectively, attenuated activity-induced nascent transcription of all tested rIEGs (Figures 3E and S3F–S3K). Taken together, we have demonstrated enhanced activity-induced BAF assembly under stringent conditions, which is insensitive to depletion of long nucleic acids.

BAF complex assembly was recently demonstrated to be modular,[14] where the ATPase forms an independent module along with SS18 (in non-neuronal cells) and finalizes complex assembly by binding to the SMARCC-containing core and ARID modules. In Figure 2E, hinting at modular assembly, BD98-mediated inhibition of ARID1A binding to SMARCC2 also prevented activity-induced enhanced binding of SMARCA4. Similarly, degradation of SMARCA4 with ACBI1, which spares both SMARCC2 and SS18L1 to various degrees, inhibited activity-induced enhanced interaction between the two (Figure

S3E). This observation suggests that SS18L1 assembles with SMARCC2 only in the presence of the ATPase, indicating a modular assembly of the complex.

Presence of nBAF is necessary for promoter-proximal RNA Pol II pausing

Prior to investigating the role of nBAF in RNA Pol II elongation, we first asked if nBAF was relevant for other aspects of the transcription cycle that precede productive elongation. Promoters of rIEGs are characterized by paused RNA Pol II near their transcription start site, which serves as a mechanism for their rapid induction.[51] Hints of a synergy between the BAF complex and RNA Pol II pausing came from our chromatin immunoprecipitation (ChIP) assays where SMARCC2 knockdown attenuated RNA Pol II enrichments near the *Arc* promoter (Figures S4A and S4B). ChIP assays were performed with two antibodies: (1) a monoclonal antibody to the N-terminal region of Rpb1, which detects total RNA Pol II independent of its phosphorylation state, and (2) a monoclonal antibody to Rpb1 CTD heptads with phosphorylation at serine 5 residues (Rpb1-pS5), which detects promoter-bound but elongation-incompetent (paused) RNA Pol II.[68] Next, we treated neurons with ACBI or BD98 for 18 h and assessed RNA Pol II subunit protein levels. Degradation or inhibition of nBAF did not alter the levels of total Rpb1 or Rpb1-pS5 (Figure S4C). However, consistent with SMARCC2 knockdown experiments, such treatments depleted paused RNA Pol II levels near the *Arc* promoter (Figures S4D–S4F). In addition to the above-mentioned pair of Rpb1 antibodies, we used an antibody against Spt5, a transcription factor known to stabilize RNA Pol II at promoter-proximal regions as part of the pausing complex.[69] Data from all three ChIP assays agreed and suggested that the presence of nBAF is necessary for maintenance of promoter-proximal RNA Pol II pausing. Interestingly, however, treatment with ACBI1 or BD98 for shorter durations (up to an hour) did not alter promoter-proximal RNA Pol II levels (data not shown). Put together, the nBAF complex—or certain subunits thereof—facilitates RNA Pol II pausing, where the facilitation process likely has a low turnover rate or nBAF is necessary for establishment of RNA Pol II pausing but not its maintenance.

Activity-induced RNA Pol II recruitment and promoter loading requires BAF subunit SMARCC2

Activity induces paused RNA Pol II to escape the promoter while also recruiting and promoter loading several additional rounds of RNA Pol II to produce a robust transcriptional output.[51,70] Prior to testing its function in elongation, we therefore verified any role of the BAF complex in activity-induced RNA Pol II recruitment and promoter loading. We performed ChIP assays with antibodies against total Rpb1, Rpb1-pS5, and SMARCC2. SMARCC2 was chosen as it is part of the BAF core module and has DNA-binding domains (SANT and SWIRM) that facilitate cross-linking and immunoprecipitation of chromatin. Neuronal activity significantly enriched Rpb1-pS5, total RNA Pol II, and SMARCC2 levels near the *Arc* promoter, which were attenuated in neurons depleted of SMARCC2 (Figures 4B–4D). SMARCC2 signal depletion after RNAi (Figure 4D) attests to the specificity of the anti-SMARCC2 antibody. Furthermore, in agreement with RNAi data, BAF complex degradation with ACBI1 attenuated activity-induced enrichment of Rpb1-pS5 and total RNA Pol II near the *Arc* promoter (Figures 4E and 4F). Unexpectedly, however, ACBI1 treatment did not affect promoter-proximal SMARCC2 enrichment (Figure 4G). Taken together, this

dataset indicates that activity-induced RNA Pol II recruitment is downstream of SMARCC2 enrichment and, as indicated by Figures 4B and 4C, is dependent on it as well. These data also lend support to an activity-dependent modular mode of nBAF assembly, where SMARCC2 independently translocates to the promoter region even when several other BAF subunits are degraded.

The nBAF complex interacts with and is regulated by the RNA Pol II EC

The purpose of activity-induced SMARCC2 translocation to the promoter region, we postulated, is to engage with the RNA Pol II EC and assemble the nBAF complex. A key EC component is P-TEFb, which signal-dependently switches RNA Pol II from a promoter-proximal paused state to productive elongation by phosphorylating, among other targets, position 2 serine residues of RNA Pol II Rpb1 CTD heptads (Rpb1-pS2).[71] To test if the BAF complex interacts with EC, we performed a coIP with CDK9, the catalytic subunit of P-TEFb. SMARCA4 and SMARCC2 were found to interact with CDK9, where the level of such interactions seemingly increased in response to activity (Figure 5A). As a control, for similar treatments, there were no changes in interactions of CDK9 with SPT6, another key member of the RNA Pol II EC.[72] Interestingly, SMARCC2 interacted with CDK9 despite ACBI1-mediated degradation of BAF subunits such as SMARCA4 (Figure 5A). This observation echoes previously stated activity-induced independent translocation of SMARCC2 to the *Arc* promoter region (Figure 4G) and suggests that CDK9-SMARCC2 may serve as the seed complex for activity-induced nBAF accretion.

To test this possibility, we performed a series of experiments. First, we catalytically inhibited CDK9 using MC180[73] or degraded it using the recently described monomeric CDK9 PROTAC (Thal-SNS-032)[74] and studied activity-induced *Arc* transcription. CDK9 has two isoforms of 55 and 42 kDa in mitotic cells, but a prominent additional faster band (~ 34 kDa) is seen in brain cells (marked as $CDK9_n$ in Figure S5A). Thal-SNS-032 treatment, which was limited to 4 h to avoid onset of apoptosis, resulted in reduced levels of two faster CDK9 isoforms (Figure S5A). Activity-induced *Arc* transcription, as expected,[51,75] was dose-dependently and highly sensitive to MC180 (catalytic inhibition) or CDK9 degradation (Figure 5B). Next, any role of CDK9 in activity-induced BAF assembly was investigated in the chromatin fraction. In response to activity, SMARCC2 displayed enhanced interaction with $CDK9_{42}$, the abundant canonical isoform known to regulate transcription (Figure S5B). Also, activity-induced enhanced interaction of SMARCC2 with ARID1A and SS18L1 was significantly attenuated upon CDK9 degradation with Thal-SNS-032 (Figures 5C–5E). This shows that the physical presence of CDK9 is necessary for activity-triggered assembly of nBAF.

Next, given that the EC travels with RNA Pol II in the gene body during productive elongation,[76] and activity induces nBAF-CDK9 association, we asked if the BAF complex also traverses the gene body during ongoing transcription. ChIP with anti-SMARCC2 revealed that, compared to control, activity induced enrichment of the subunit in the *Arc* gene body (Figure 5F). Attesting to signal specificity, such enrichment was not seen in neurons depleted of the subunit. Similar SMARCC2 enrichment was also recorded in five additional IEGs (Figures S5C–S5G). Next, we treated neurons with CDK9 inhibitors

(flavopiridol and MC180). As expected, elongation-competent Rpb1-pS2 levels increased in the *Arc* gene body in response to activity but dropped to baseline in response to CDK9 inhibitors (Figure 5G). Similarly, activity-induced enrichment of SMARCC2 in the gene body was also sensitive to CDK9 inhibition (Figure 5H).

To correlate productive elongation with the BAF complex, we investigated the latter's role on activity-induced RNA Pol II elongation rate. Here, we utilized the 5,6-dichlorobenzimidazole (DRB) protocol, where transcription is blocked for an hour with DRB followed by its washout to induce synchronized gene transcription without external stimuli.[77,78] DRB washout induced rapid transcription of *Arc* pre-mRNA, whose elongation rate improved over time (Figure S5H). However, the rate of elongation in BD98-treated neurons was significantly less at all tested time points (Figure S5H). Taken together, datasets in Figures 5 and S5 suggest that the BAF complex likely accompanies the EC through the gene body during productive elongation and facilitates the latter.

The nBAF complex interacts with elongation-competent RNA Pol II

If the BAF complex is to have a regulatory role in transcription elongation, its signal-dependent interaction with elongation-competent RNA Pol II is highly likely. We tested this possibility by performing coIP with an antibody against Rpb1-pS2. Interactions between Rpb1-pS2 and SMARCC2 (and other BAF complex subunits) increased in response to activity (Figures 6A and 6B). This enhanced interaction was sensitive to BD98 (Figures 6A and 6B), which prevents induced nBAF assembly. To test for such association in stringent conditions, we performed coIP with an antibody against SMARCC2 in the chromatin fraction. Here, association of SMARCC2 with elongation-competent RNA Pol II increased after activity in a BD98-sensitive fashion (Figures 6C and 6D). To test if the BAF complex could be detected within the gene body during active transcription, we performed ChIP. Activity significantly enriched SMARCC2 levels in the *Arc* gene body (Figure 6E), which aligns with our coIP data above that demonstrate interactions of the nBAF complex with the EC and elongation-competent RNA Pol II. Such activity-induced SMARCC2 gene body enrichment was sensitive to the nBAF inhibitor BD98 and BAF degrader ACBI1 (Figure 6E). Notably, activity-induced SMARCC2 enrichment was differentially susceptive to ACBI1 at the *Arc* promoter (insensitive; Figure 4G) versus in the gene body (sensitive). Together, data presented so far suggest a promoter-proximal modular assembly of nBAF, followed by its participation in RNA Pol II productive elongation.

Assembled complex and its ATPase activity are required for productive elongation

To decouple the role of nBAF in productive elongation from its involvement in RNA Pol II recruitment and initiation at the promoter, we used triptolide. Triptolide is an inhibitor of the ATPase activity of XPB, the transcription factor IIH (TFIIH) heli-case/translocase subunit found in the transcription initiation complex. Triptolide treatment prevents new transcription initiation but does not interfere with promoter escape and productive elongation of paused RNA Pol II.[37,79,80] To verify its effect on *Arc* transcription, we treated neurons with triptolide and subjected them to activity. Transcription was significantly induced in triptolide-treated neurons but, as expected due to obstructed RNA Pol II initiation, was less compared to the full-bodied transcription in counterpart neurons without the

inhibitor (Figure 7A). Strong induction despite XPB/TFIIH inhibition indicates the ability of promoter-proximal paused RNA Pol II to enter productive elongation signal dependently. Such initiation-independent elongation was next studied after inhibiting induced nBAF assembly (BD98) or its ATPase activity (BRM014). Both BD98 and BRM014 significantly reduced initiation-decoupled *Arc* transcription (Figure 7A). These data strongly suggest that the nBAF complex is necessary for productive elongation of *Arc*.

To corroborate the relationship of nBAF and RNA Pol II elongation further, we performed a series of ChIP assays focusing on the *Arc* gene body. First, we assayed for SPT6, a representative of the EC. SPT6 levels significantly increased in response to activity, both in the absence and in the presence of triptolide, albeit less so in the latter (Figure 7B). Echoing gene transcription trends seen in Figure 7A, such activity-induced SPT6 gene body enrichment was attenuated when neurons were also treated with BD98 (Figure 7B). Next, two sets of ChIP assays were performed with and without triptolide using antibodies against total Rpb1 and elongation-competent Rpb1-pS2. Total Rpb1 near the promoter was used to normalize amounts of Rpb1 and Rpb1-pS2 in the gene body. This normalization was necessary because activity-induced promoter-proximal Rpb1 levels differed in the presence of triptolide (Figures 7C and 7F). When normalized as above, levels of Rpb1 and Rpb1-pS2 in the gene body were comparable in neurons with and without triptolide. Also, their levels were significantly more after activity versus control (Figures 7D, 7E, 7G, and 7H). To unveil underlying mechanisms, neurons were also treated with BD98 to block nBAF assembly and BRM014 to inhibit ATPase activity during initiation-decoupled elongation. Both small-molecule interventions attenuated activity-induced enrichment of Rpb1 and Rpb1-pS2 in *Arc* gene body (Figures 7D, 7E, 7G, and 7H), demonstrating that productive elongation of RNA Pol II in the *Arc* gene body requires activity-induced assembly of nBAF and its ATPase activity.

Finally, to broaden the scope of nBAF function in rIEG transcriptional elongation and to rule out the above observations being only an *Arc*-specific phenomenon, we extended the ChIP assay to five additional rIEGs (*cFos*, *Gadd45g*, *Cyr61*, *Btg2*, and *Dusp1*), which displayed sensitivity to ACBI and BD98 (Figures S1 and S3). The trend of Rpb1-pS2 levels in the body of these genes was as seen in *Arc*; levels increased after Bic + 4AP treatment and activity, remained comparable (or decreased somewhat) if elongation was isolated from initiation, but dropped significantly if nBAF assembly was inhibited with BD98 along with initiation-elongation decoupling (Figure S6). Taken together, our data demonstrate that nBAF regulates productive elongation in rIEG gene bodies via interaction with the EC and elongation-competent RNA Pol II, which is mechanistically mediated by activity-induced assembly and its ATPase activity.

DISCUSSION

This study contributes the following observations: (1) neuronal activity induces nBAF assembly, (2) activity-assembled nBAF mediates RNA Pol II productive elongation, and therefore, (3) nBAF is necessary for activity-induced rIEG transcription.

The BAF complex is often thought of as a developmentally assembled polymorphic complex, which undergoes a cell-type-specific compositional transformation in neurons, referred to as the nBAF.[18] It remained unknown if nBAF is a steady-state complex that remains compositionally impervious to neuronal activity or if it can undergo recurring rounds of complex formation, especially in response to transcriptional profile-altering cellular signals. Here, we show that neuronal activity induces ancillary assembly of nBAF on top of its basal level (Figure 2E). Our data indicate that such assembly is ordered and modular in nature. Modular assembly of BAF complex was recently described,[14] where complex formation is initiated by the SMARCC1/SMARCC2 core module. This core binds next to the subunit-defining ARID1 module, which then binds to the BRG1/BRM- and SS18/L1-containing ATPase module to finalize the assembly. The following observations led us to believe that activity-induced neuronal nBAF assembly is similarly modular: (1) inhibition of ARID1A-SMARCC2 binding with BD98 also attenuates SMARCA4-SMARCC2 association (Figure 2E), (2) SS18L1 assembles with SMARCC2 only in the presence of the ATPase (Figure S3C), and (3) SMARCC2 is independently recruited to the *Arc* promoter region and binds to EC (CDK9) despite ACBI1-dependent depletion of SMARCA4 (Figures 4G and 5A). Furthermore, during the preparation of this article, an independent study in preprint[81] demonstrated activity-induced enhanced interaction of SMARCA4 with ARID2. Considering that study together with our study, it is possible that membrane depolarization induces assembly of both nBAF and PBAF, which then undertake independent and overlapping functions to mediate the span of nuclear responses to activity.

The relationship between the BAF complex and RNA Pol II has been studied over the years in many models and cell types. These studies include genome-wide studies where ChIP with high-throughput sequencing (ChIP-seq) and other global approaches suggest that BAF subunits largely enrich at gene promoters and enhancers, where they facilitate functions of these genomic regions.[33,37,82–87] From these studies, the BAF complex may be inferred to have promoter- and enhancer-specific functions only. RNA Pol II elongation, being dynamic and non-synchronous in a cell population, can be elusive to capture with global techniques such as ChIP-seq of BAF subunits. Therefore, we approached the issue using rIEGs at an early time point where paused RNA Pol II release, rather than recruitment, primarily mediate transcriptional changes. Such instances lend themselves well to decoupling of productive elongation from RNA Pol II recruitment and initiation via small-molecule pharmacology (e.g., triptolide). Our triptolide assays with *Arc* and other rIEGs (Figures 7 and S6) clearly show the necessity of nBAF during productive elongation. During elongation, the nBAF complex works in conjunction with the EC, perhaps boosting each other's functions. Whether nBAF is also responsible for RNA Pol II elongation in other longer genes remains to be investigated in the future with genome-scale approaches such as mammalian native elongating transcript sequencing (NET-seq),[88] a powerful technique that still needs optimization in non-dividing cells such as neurons.

In lieu of its role in RNA Pol II elongation, nBAF is necessary for activity-induced transcription of rIEGs. This inference is drawn from our above studies that utilized RNAi against two BAF subunits, two degraders of various BAF complexes, and inhibitors of nBAF assembly or its catalytic activity. However, our findings appear to contradict a previous study,[89] which reported that loss of the neuron-specific BAF subunit ACTL6B derepresses

rIEGs. There are several avenues to reconcile the apparent differences in our conclusions. One, compared to our inhibitors and degraders that work in minutes to hours, RNAi and knocking out a target in animals—as used by the previous study—deplete the protein of interest over days. Such longer durations leave room for cellular homeostatic mechanisms (e.g., retention of the non-neuronal paralog ACTL6A instead[89]) to influence the outcome. Such possibilities are supported by our observation in Figure 1, where ACBI1 treatment for 3 h degraded ACTL6B but did not derepress rIEG transcription. Two, ACTL6A is a constituent of cBAF, PBAF, and GBAF. It is possible that ACTL6B, the neuronal paralog, similarly convenes with all three BAF complexes in neurons and the reported phenotypic outcome of its loss is underwritten by one or more malfunctioning BAF complexes. Taken together, the role of BAF complex in activity-induced rIEG is nuanced, where complex subtype and its composition likely play complementary or contradictory roles in a context-dependent fashion. To comprehend such a nuanced set of functions elaborately, future work must be directed to distinct BAF subcomplexes.

Our current findings will be relevant to several human disorders and diseases that, on one hand, are associated with inefficient gene transcription, especially aberrant productive elongation, and on the other hand, correlate with mutations in genes encoding BAF subunits. For example, among non-neuronal cells, many forms of cancer stem from defective RNA Pol II elongation.[90–92] Many of these cancers also prominently feature mutations in BAF genes.[93] In the brain, anomalies of RNA Pol II elongation have been implicated in NDDs[94] and brain cancers.[95] With regard to NDDs—"BAFopathies"— genes coding for cBAF subunits possess the most *de novo* missense and protein-truncating mutations among all nuclear protein complexes.[28] Also, biallelic mutations in the neuron-specific *ACTL6B* or haploinsufficiency of *ARID1B* causes recessively inherited autism,[24,89] microduplication of *ARID1A* causes ID,[96] and *SMARCC2* is a high-confidence autism gene.[97–101] As for brain tumors, *SMARCA4* is recurrently mutated in multiple cancers.[102] Future studies are expected to reveal cause-effect association between these mutations, RNA Pol II elongation defects, and human maladies.

Limitations of the study

Here, we demonstrate that nBAF is signal-dependently assembled, which then allows the complex to interact with the EC and mediate RNA Pol II activities at gene promoters and gene bodies. Association with the EC likely is part of a larger web of interactions that include elongation-competent RNA Pol II. However, this study does not illuminate such a web in its entirety, nor does it test the role of CDK9-modified elongation-competent RNA Pol II in nBAF recruitment and assembly. It remains unclear if the nBAF complex is a steady-state constituent of the EC or an intermittent participant that aids the elongation process to overcome nucleosomal barriers and/or undertake co-transcriptional splicing. It also remains to be investigated if PBAF and/or GBAF undertakes a synergistic role in activity-induced IEG transcription or that of other longer genes implicated in human disorders. Among these longer genes, it will be of interest to investigate if BAF complexes have unique or redundant roles in regulating RNA Pol II velocity and its passage through chromatin barriers. Last, but not the least, this study was performed in dissociated cells. We look forward to further development of BAF complex inhibitors and degraders to make them

blood-brain barrier permeative, which will then allow extension of our current enquiries into the brain.

RESOURCE AVAILABILITY

Lead contact

Requests for further information and resources and reagents should be directed to and will be fulfilled by the lead contact, Ramen Saha (rsaha3@ucmerced.edu).

Materials availability

The study did not generate new mouse lines or unique reagents.

Data and code availability

- The mass spectrometry raw data files and MSFragger search results have been deposited in the jPOST database (https://repository.jpostdb.org/) and can be accessed via dataset identifier JPST003157 for jPOST and PXD052840 for ProteomeXchange.
- This paper does not report original code.
- Any additional information required to reanalyze the data reported in this paper is available from the lead contact upon request.

STAR★METHODS

EXPERIMENTAL MODEL AND STUDY PARTICIPANT DETAILS

This study used primary cultures of cortical neurons prepared from embryonic day 18 rat pups (IACUC approval, AUP 2022-1143, University of California, Merced). Brains were collected from pups from both sexes and mixed in a homogenous population of dissociated cells. Details: Experiments were performed using dissociated cortical rat neurons obtained from Sprague-Dawley rats as previously published[54]. Time-pregnant rats were purchased from Charles River Laboratories. Rats were delivered (E18) 2 days prior to dissection and housed individually on a 12-hour light/dark cycle with access to food and water *ad libitum*. Dams were anesthetized with Euthasol® (390 mg/ml sodium pentobarbital and 50 mg/ml sodium phenytoin) and decapitated using a guillotine. Embryonic day 18 pups were removed and used to prepare primary cultures of cortical neurons under animal protocol #22-1143, reviewed and approved by the University of California, Merced IACUC. To remove cortical hemispheres, heads were cut and transferred to a plate containing HBSS plus $Ca^{2+}$and Mg^{2+} (Gibco, catalog no. 14025092). A medial cut was made caudal to rostral of the head and gently pushed the brain out without disturbing the cortex. Under a dissecting microscope, the brain was placed with the ventral surface facing upwards, a cut was made in the sagittal plane to separate the hemispheres. Meninges were then carefully removed thoroughly. The collected tissue was placed in a dish containing HBSS plus $Ca^{2+}$and Mg^{2+} (Gibco, catalog no. 14025092) and taken to a tissue culture room for mechanical dissociation. 1 milliliter of StemPro® Accutase® (Life Technologies, Inc., catalog no. A1110501) was added for a 7-minute digestion, followed by mechanical dissociation with fire-polished Pasteur pipettes.

The reaction was stopped by adding 5 milliliters of HBSS lacking $Ca^{2+}$and Mg^{2+} (Gibco, catalog no. 14175095). The dissociated neuron resuspension was then centrifuged for four minutes at 200 rcf, resuspended in plating media, and used to do a cell count. Cell counts were done using trypan blue and a TC20TM automated cell counter (Bio-Rad, catalog no. 1450102), and subsequently plated to dishes containing pre-warmed Neurobasal medium (Gibco, catalog no. 21103049) supplemented with 25 μM glutamate (Sigma- Aldrich, catalog no. 1446600), 0.5 mM L-glutamine (Sigma-Aldrich, catalog no. G8540). 100 cm2 dishes were plated at a density of 7.8×10^6 neurons or 35 cm2 dishes at a density of 1.0×10^6. Cells were maintained at 37°C in a humidified incubator with 5% CO2. Neurons were grown for up to two weeks in the medium described above without glutamate, replacing half the media every 3– 4 days. Matured neurons were then used for various assays between 10–14 days.

METHOD DETAILS

Pharmacological treatments—Neuronal activity was induced by co-treating neurons with 50uM Bicuculline (Sigma-Aldrich, catalog no. 14340) and 75 μM 4-aminopyridine (Acros Organics, catalog no. 104571000). This treatment is noted as Bic+4AP throughout the manuscript. To degrade BAF complex, neurons were treated with ACBI1 (OpnMe). 1μM or 2.5μM ACBI1 were used for Western blot analysis and RNA assays. 2.5 μM ACBI1 dose was used for ChIP assays. Cells were pre-treated for 3 hours. SMARCA4 protein degradation was used as a control to assess ACBI1 efficiency. cisACBI1 (OpnMe) was used as negative control. To inhibit BAF ATPase function, BRM014 (compound 14, MedChemExpress; catalog no. HY-119374) and FHT-1015 (MedChemExpress; catalogue no. HY-144896) were used at concentrations described in figure legends. BD98 (BRD-K98645985), BRD7i 2–77 (PBAF inhibitor), BRD9i (GBAF inhibitor), and VZ-185 (PBAF and GBAF degrader) were obtained from the Dykhuizen lab. BD98 is now commercially available from MedChemExpress (catalogue no. HY-114268). BRD7i, BRD9i, and VZ-185 are commercially available from OpnMe. Cells treated with BRM014, FHT-1015, BD98, BRD7i 2–77, or BRD9i were pre-treated for 15–30 mins at concentrations indicated in figures, with or without Bicuculline+4AP added in the last 15 minutes of the treatment. VZ-185 (0.25 μM) was pre-treated for three hours with or without Bicuculline+4AP added in the last 15 minutes. Brd7 and/or Brd9 protein degradation was used as a control to assess VZ-185 efficiency. To inhibit phosphorylation of RNA Pol II CTD (pS2), MC180295 and Flavopiridol were used at indicated concentrations. Cells were treated for 20 minutes with the inhibitors, which was followed by 15 minutes of induced neuronal activity with Bicuculline+4AP. To degrade CDK9, PROTAC Thal-SNS032 was used. Cells were pre-treated for 3 hours with or without induced neuronal activity with Bicuculline/4AP. RNA assays utilized 1μM or 2.5 μM final concentrations. Co-IP cell treatments used 2.5 μM final concentrations. CDK9 protein degradation was used as a control to assess Thal-SNS032 efficiency.

Co-immunoprecipitation (Co-IP)—After performing treatments as indicated, neurons were lysed in 335uL of IP buffer (5–10% Ficoll; 1mL glycerol; 150mM NaCl; 20 mM Tris–HCl [pH 7.5]; 1.25 mM EGTA; 2 mM EDTA; 0.05% Tween-20). Protease/phosphatase inhibitor cocktail was added as recommended. Cells were lysed 8–12 times with a 1.5 inch

26-gauge needle and sheared by sonication (8 × 30s, HIGH setting in Bioruptor®). Sonicated material was centrifuged at 15,000 rpm for 1 min at 4°C to clear debris. Antibodies (1–4μg) were pre-loaded on A/G beads for 30 minutes at 35°C and 5–20% inputs were set aside for each treatment. Sonicated material and preloaded magnetic A/G beads (Pierce) were pulled down for 2 hours at 35°C with constant rotation. A/G bead-protein complexes were prepared for gel electrophoresis by resuspending in sample buffer (4X Laemmli sample buffer with 10% b-mercaptoethanol; diluted to 1X with IP buffer) and heating at 95°C for 3–5 minutes. Beads were separated on a magnetic rack and processed samples were electrophoresed. Co-IP assays were performed in 4+ biological replicates.

Gel electrophoresis and western blotting—Neurons were lifted from cell culture dishes with sonication buffer (20 mM Tris–HCl [pH 8]; 1.25 mM EGTA; 2 mM EDTA; 0.5% SDS) supplemented with 1:100 protease/phosphatase inhibitor cocktail (Cell Signaling; catalog no. 5872S). Lysates were sheared by sonication (4–8X cycles of 30s, HIGH setting in Bioruptor®). Sonicated material was centrifuged at 15,000 rpm for 1 min at 4 °C to clear debris. Samples were combined with (4X Laemmli sample buffer; Bio-Rad; catalog no. 1610747) with 10% b-mercaptoethanol (Sigma; catalog no. 63689) and were warmed for 10 min at 95°C in a heat block. Sample and dye mixtures were then loaded in a 4–20% (Bio-Rad; catalog no.: 4568095) or 4–15% (Bio-Rad; catalog no.: 456-1083) gels. After electrophoresis at 90–100V, gels were transferred to a polyvinylidene difluoride (PVDF) membrane (Bio-Rad; catalog no. 10026933) using the Bio-Rad Trans-Blot Turbo Transfer System with 20% Methanol-containing transblot turbo transfer buffer (Bio-Rad; catalog no. 10026938) for 10–15 minutes. PVDF membranes were immediately transferred to cold Tris-buffered saline with Tween-20 (TBS-T 0.1%) and incubated at 4°C overnight in primary antibody solution [0.1% TBS-T supplemented with 3% BSA (Fisher; catalog no.: BP9703) and protease-phosphatase inhibitors]. Membranes were washed three times every 5 minutes in 0.1% TBS-T before being probed with secondary antibody for 60 minutes at room temperature. Secondary antibodies were either goat-anti–mouse 647 (RRID: A21236) or goat-anti–rabbit 488 (RRID: A11034) Alexa Fluor secondary antibodies (Life Technologies). Membranes were washed three times with 0.1% TBS-T for 5 min each and imaged using Bio-Rad Multiplex ChemiDoc Imaging System. Densitometric quantifications were performed in ImageLab Software 2020. Displayed images are marked for molecular weight markers. Removal of any unrelated intermediate lanes are marked by a thin vertical line on the blot display.

Chromatin fractionation—Treatments were performed as outlined in the figure legends and cells were separated into fractions to extract the chromatin. This protocol was adapted and modified from published protocols by the Churchman group[66,67]. To start, 7.8×10^6 cells were scraped and collected by centrifugation at 350g for two minutes. Cells were resuspended in 500μL of Cytoplasmic Lysis Buffer [10mM Tris-HCl pH 7.0; 150mM NaCl; 0.15% %(vol/vol) NP-40; protease inhibitor 1x]. The cell lysate mixture was then incubated on ice. While the incubation occurred, 700μL of sucrose buffer [10mM Tris-HCl pH 7.0; 150mM NaCl; 15% (wt/vol) filter-sterilized sucrose; protease inhibitor 1x] was added to a clean 1.5mL microcentrifuge tube in preparation for the next step. The 500 μL cell lysate was carefully layered onto the sucrose buffer and centrifuged at 16,000g for 15 minutes

at 4°C. The supernatant was removed, and the nuclei remained as a soft pellet that was carefully washed with 800μL of Nuclei Wash Buffer [0.1% (vol/vol) Triton-X-100; 150mM NaCl; 1mM EDTA; protease inhibitor 1x]. Washed nuclei were then centrifuged at 1,150g for one minute. To isolate the chromatin fraction, washed nuclei were resuspended in 200μL of Glycerol Buffer [20mM Tris-HCl pH8.0; 75mM NaCl; 50% (vol/vol/) filtered-sterilized glycerol; .5mM EDTA; .85mM DTT; protease inhibitor 1x]. Then, 200μL of Nuclei Lysis buffer [20mM HEPES pH 7.5; 300mM NaCl; 1% (vol/vol) NP-40; .2mM EDTA; 1mM DTT; 1M urea; protease inhibitor 1x] was layered onto the resuspended nuclei and mixed by pulsed vortexing. After a 2-minute incubation on ice, the lysed nuclei were centrifuged at 18,500g for 2 minutes. Supernatant was removed and the remaining pellet is the chromatin fraction. Subsequently, the chromatin fraction was utilized for Co-IPs (resuspended in 150 μL of IP buffer) or for extracting nascent RNA resuspended in 50 μL of Chromatin Resuspension Buffer (PBS; protease inhibitor 1x).

Nuclear extract preparation with high salt—Mature neurons were treated, collected, and centrifuged at 300 RCF. The cell pellet was resuspended in 1 mL of Buffer A (160 mM KCl, 1.5 mM MgCl2, 0.1% NP40 wt/vol, and 0.5 mM DTT) and rotated at 4°C for five minutes, followed by a pulse vortex. The suspension was centrifuged at 3000 RCF, supernatant was discarded, and the cells were resuspended in 200 μL of Buffer B (50 mM Tris pH 8.0, 1% NP-40, and 0.25% sodium deoxycholate, protease phosphatase). The cells were kept on ice for five minutes, then NaCl was added to a final concentration of 300 mM. The cells were placed on ice for three minutes and centrifuged at 6000 RCF for five minutes. The supernatant was carefully collected to avoid any chromatin contamination. The samples were then used in downstream assays.

Mass spectrometry sample preparation—Each sample received 50 μL of Phase Transfer Surfactant (PTS) lysis buffer, which included 12 mM SDC, 12 mM SLS, 50 mM Tris-Cl (pH 8.5), 10 mM TCEP, and 40 mM CAA. Phosphatase inhibitor was added at a 1x concentration. Samples were incubated with 50 μL of the PTS buffer and boiled for 10 minutes at 95°C with shaking at 1200 RPM. After boiling, samples were adjusted to 70% acetonitrile by adding 135 μL of 100% ACN, mixed, and incubated for 10 minutes at room temperature to precipitate proteins onto the beads. The beads were then washed three times in fresh 95% acetonitrile and twice in fresh 70% ethanol, each wash consisting of 2.5 minutes on a magnet with 300 μL of wash solution. On-bead digestion was carried out by adding 1 μg lys-C/trypsin mix at a ratio of 1 μg trypsin per 50 μg proteins in 50 μL of 100 mM TEAB and incubating at 1200 RPM overnight. The supernatant was separated from the beads, and the beads were washed with 40 μL of 0.1% TFA. The supernatant and wash were combined, and 10% TFA solution was added to achieve a final concentration of 1% TFA. For desalting, TopTip C-18 columns (10–200 μL, Glygen, Part number: TT2C18.96) were used. TopTips were spun down at 500 × g for 2 minutes and washed twice with 100 μL of 0.1% TFA in 80% ACN, centrifuged at 500 × g for 1 minute, and acidified by washing three times with 100 μL 0.1% TFA aqueous solution, followed by centrifugation at 500 × g for 1 minute. The sample concentration was adjusted with 10% TFA aqueous solution to achieve a final 0.1% TFA concentration. Samples were added to the columns and centrifuged at 200× g for 3 minutes. Each column was washed three times using 100 μL 0.1% TFA

aqueous solution, with centrifugation at 500 × g for 1 minute between washes. The elution of peptides was done by transferring columns to new tubes, adding 100 µL of 0.1% TFA in 80% ACN, centrifuging at 200 × g for 1 minute, and repeating this step to collect 200 µL of desalted peptide samples. Ten percent of the samples were dried completely for the peptide colorimeter assay, and the peptide concentrations were measured at 480 nm using a plate reader. Finally, approximately 1 µg of samples were completely dried and loaded onto Evotips by resuspending them in Buffer A.

LC-MS/MS—Peptide mixtures loaded onto Evotips were analyzed using an Evosep One HPLC system coupled to a timsTOF HT mass spectrometer (Bruker). An 8cm × 150µm reverse-phase column packed with 1.5 µm C18-beads (PepSep) was used. The analytical column was connected with a fused silica emitter (20 µm diameter; Bruker Daltonics) inside a nanoelectrospray ion source (Captive Spray source; Bruker). The timsTOF HT was operated in positive polarity and data-dependent acquisition (DDA)-PASEF scan mode. The DDA-PASEF method covering an m/z range from 100 to 1700 was utilized. The IM range was set to 1.3 to 0.7 V-s cm-2. The accumulation and ramp times were specified as 100 ms with 10 PASEF ramps and a charge maximum of 5. As a result, the DDA-PASEF method has a cycle time of 1.17 s. The target intensity was set to 20,000, the intensity threshold was set to 2,500, the measuring time was set to 2.75 ms, and the switching time was set to 1.65 ms. The collision energy was decreased as a function of the IM from 59 eV at 1/K0 = 1.6 V-s cm-2 to 20 eV at 1/K0 = 0.6 V-s cm-2, and the IM was calibrated with three Agilent ESI Tuning Mix ions (m/z, 1/K0 = 622.03, 0.99 V-s cm-2, 922.01, 1.20 V-s cm-2, 1221.99, and 1.39 V-s cm-2).

Mass spectrometry data analysis—The signal extraction and quantitation of the DDA data were performed in FragPipe v20.0 (MSFragger v3.8, IonQuant v1.9.8, and Philosopher v.5.0.0), utilizing a standard setting with some modifications. The “d” files were analyzed together in a FragPipe session. Specific digest types with strict trypsin enzyme, 7 minimal peptide length, 50 maximum peptide length, carbamidomethyl at cysteine as fixed modification, acetyl protein N-term and oxidation at methionine as variable modifications, phosphorylation at serine, threonine, and tyrosine when applicable, and 3 as maximum variable modifications were used. DDA “d” files were searched against the human protein sequence database. The FDR at PSM, peptide, and protein group were set to 0.01. The IonQuant feature was enabled with MaxLFQ (2 min ions), match between runs, and normalize intensity across runs.

Abundance levels (MaxLFQ Intensity) were extracted from the MSFragger (combined_protein.txt). These abundances were normalized to Smarcc2, ensuring that all Smarcc2 values in the six samples equaled 1. The abundances were then log2 transformed. For grouping, the transformed abundances were categorized into each group (M or B). Proteins with a maximum of 0% missing values in at least one group were retained, allowing for the inclusion of proteins consistently quantified in either category (M or B) and the exclusion of those with many missing values. Missing abundance values were imputed using small random values from a normal distribution, typically due to very low abundances. Subsequently, an unpaired two-tailed Student’s t-test was performed, and the difference

in log2 fold-change on averages was calculated. From this t-test, we obtained p-values, q-values (FDR), and the log2 fold-change difference for each phosphopeptide. Volcano plots were generated in R using the EnhancedVolcano package (version 1.16.0) with p-value < 0.05 and difference thresholds >0.0 and <0.0 (Fold change = 2^Difference).

Chromatin immunoprecipitation (ChIP)—Neurons were cross-linked with 1% formaldehyde for 5 minutes after indicated treatments. Crosslinking reaction was quenched for 5 minutes with 1.25 M glycine buffer in PBS. Cross-linked cells were resuspended in sonication buffer (20 mM Tris–HCl [pH 7.5]; 1.25 mM EGTA; 2 mM EDTA; 0.5% SDS, supplemented with inhibitors for proteases and phosphatases, 1:100) followed by sonication for 16 cycles (bursts and intervals of 30s each) with the Bioruptor® (Diagenode), which produced 200–1000 bp genomic DNA fragments. Sonicated samples were then immunoprecipitated overnight at 4°C in IP buffer with 2–5μg antibody. 20% of the sonicated material was set aside for inputs. Antigen-antibody complexes were immunoprecipitated with Pierce Protein A/G Magnetic Beads, washed four times with low salt buffer, once with LiCl buffer, and finally once with Tris-EDTA. Samples were reverse cross-linked at 65°C degrees overnight, and chromatin DNA was eluted using the Thermo Scientific™ GeneJET Plasmid Maxiprep Kit. Eluted chromatin was quantified by qPCR. Heat map in Figure S3 was generated using ChIP material used figure 7C–E. Primers against promoter and gene body (~1000 bp downstream of TSS) of five rIEGS were used to create the heat map. In summary, total Rpb1 near the promoter was used to normalize amounts Rpb1-pS2 in the gene body for each treatment. Heat map depicts the mean value of N=3 with a baseline-correction (baseline is the Media treatment) calculated as a percentage (100 * (value/baseline).

RNA-based pre-mRNA quantification assays—Total RNA was extracted using the RNAspin Mini kit (GE Lifesciences; catalog no. 25050072) following the manufacturer's instructions. RNA processing, PCR amplification and quantification has been previously described in publications from our lab[55,77]. The Bio-Rad CFX Connect real-time PCR Detection System was used here.

Cellular thermal shift assay (CETSA)—CETSA was adapted from Jafari *et. al.*[60] Briefly, neurons were treated with BD98 (20 μM) or DMSO as a control. Cells were scraped, collected in 0.5ml of media, and centrifuged at 500 rcf. Supernatant was removed and cells were resuspended in 0.5ml of 1x PBS. For each treatment, cell lysate was split, and a portion was added to PCR tubes. Each tube was individually subjected to a unique temperature. We initially tried a temperature range of 37°C – 47°C and found BAF subunits degrading sufficiently at 43.3°C. Samples were exposed to 37°C or 43.3°C temperate for three minutes, then left at room temperature for an additional three minutes. Then samples were frozen for 12 minutes at −80 degrees, fast thawed, and frozen again. After freeze/thawing, samples were placed on ice and transferred to clean. Transferred lysates were centrifuged at 15000 rpm for 20 minutes at 4°C to remove debris and the supernatant was prepared for Western blot analysis.

RNAi—SMARCC2 shRNA is previously published by our lab[58]. The shRNA construct for ARID1A (target sequence: TGGACCTCTATCG CCTCTATG, NM_006015) was obtained from Sigma (TRCN0000358749). This pLKO.1-based construct was packaged into lentiviruses. Self-inactivating HIV lentivirus particles were produced by transfecting 293 T cells with the shRNA vector, envelope (pMD2.G; Addgene), and packaging plasmids (psPAX2; Addgene) using a previously described protocol[51]. Efficiency of this construct was validated by Western blotting for ARID1A.

QUANTIFICATION AND STATISTICAL ANALYSIS

Statistical analyses were conducted using GraphPad Prism 10 (GraphPad software, San Diego, CA). Error bars represent standard error of the mean. No tests for outliers were conducted; therefore, all data points were included. Effects were determined by t test or one-way ANOVA with appropriate *post hoc* tests for determination of *P* values; details are indicated in the figure legends. Biological replicates are indicated throughout within figures or in their legends. Biological replicates constitute cell culture preparations from the pooled cortices of embryos from independent dams.

Supplementary Material

Refer to Web version on PubMed Central for supplementary material.

ACKNOWLEDGMENTS

Technical support from Mariam Doss, Baani Minhas, Courtny Nimez, and Isabel Ramos is gratefully acknowledged. This study was funded by the following National Institutes of Health grants: (1) from the National Institute of Environmental Health Sciences (NIEHS) to R.N.S. (R01ES028738) and (2) from the National Institute of Mental Health (NIMH) to R.N.S and E.C.D. (R21MH128678).

REFERENCES

1. Stern M, Jensen R, and Herskowitz I (1984). Five SWI genes are required for expression of the HO gene in yeast. J. Mol. Biol 178, 853–868. 10.1016/0022-2836(84)90315-2. [PubMed: 6436497]
2. Cairns BR, Kim YJ, Sayre MH, Laurent BC, and Kornberg RD (1994). A multisubunit complex containing the SWI1/ADR6, SWI2/SNF2, SWI3, SNF5, and SNF6 gene products isolated from yeast. Proc. Natl. Acad. Sci. USA 91, 1950–1954. 10.1073/pnas.91.5.1950. [PubMed: 8127913]
3. Neigeborn L, and Carlson M (1984). GENES AFFECTING THE REGULATION OF SUC2 GENE EXPRESSION BY GLUCOSE REPRESSION IN SACCHAROMYCES CEREVISIAE. Genetics 108, 845–858. 10.1093/genetics/108.4.845. [PubMed: 6392017]
4. Dingwall AK, Beek SJ, McCallum CM, Tamkun JW, Kalpana GV, Goff SP, and Scott MP (1995). The Drosophila snr1 and brm proteins are related to yeast SWI/SNF proteins and are components of a large protein complex. Mol. Biol. Cell 6, 777–791. 10.1091/mbc.6.7.777. [PubMed: 7579694]
5. Wang W, Côté J, Xue Y, Zhou S, Khavari PA, Biggar SR, Muchardt C, Kalpana GV, Goff SP, Yaniv M, et al. (1996). Purification and biochemical heterogeneity of the mammalian SWI-SNF complex. EMBO J. 15, 5370–5382. 10.1002/j.1460-2075.1996.tb00921.x. [PubMed: 8895581]
6. Wang W, Xue Y, Zhou S, Kuo A, Cairns BR, and Crabtree GR (1996). Diversity and specialization of mammalian SWI/SNF complexes. Genes Dev. 10, 2117–2130. 10.1101/gad.10.17.2117. [PubMed: 8804307]
7. Alpsoy A, and Dykhuizen EC (2018). Glioma tumor suppressor candidate region gene 1 (GLTSCR1) and its paralog GLTSCR1-like form SWI/SNF chromatin remodeling subcomplexes. J. Biol. Chem 293, 3892–3903. 10.1074/jbc.RA117.001065. [PubMed: 29374058]

8. Centore RC, Sandoval GJ, Soares LMM, Kadoch C, and Chan HM (2020). Mammalian SWI/SNF Chromatin Remodeling Complexes: Emerging Mechanisms and Therapeutic Strategies. Trends Genet. 36, 936–950. 10.1016/j.tig.2020.07.011. [PubMed: 32873422]

9. Phelan ML, Sif S, Narlikar GJ, and Kingston RE (1999). Reconstitution of a core chromatin remodeling complex from SWI/SNF subunits. Mol. Cell 3, 247–253. S1097-2765(00)80315-9 [pii]. [PubMed: 10078207]

10. Lessard J, Wu JI, Ranish JA, Wan M, Winslow MM, Staahl BT, Wu H, Aebersold R, Graef IA, and Crabtree GR (2007). An essential switch in subunit composition of a chromatin remodeling complex during neural development. Neuron 55, 201–215. S0896-6273(07)00452-7 [pii]. [PubMed: 17640523]

11. Nguyen H, Sokpor G, Pham L, Rosenbusch J, Stoykova A, Staiger JF, and Tuoc T (2016). Epigenetic regulation by BAF (mSWI/SNF) chromatin remodeling complexes is indispensable for embryonic development. Cell Cycle 15, 1317–1324. 10.1080/15384101.2016.1160984. [PubMed: 26986003]

12. Narayanan R, Pirouz M, Kerimoglu C, Pham L, Wagener RJ, Kiszka KA, Rosenbusch J, Seong RH, Kessel M, Fischer A, et al. (2015). Loss of BAF (mSWI/SNF) Complexes Causes Global Transcriptional and Chromatin State Changes in Forebrain Development. Cell Rep. 13, 1842–1854. 10.1016/j.celrep.2015.10.046. [PubMed: 26655900]

13. Ronan JL, Wu W, and Crabtree GR (2013). From neural development to cognition: unexpected roles for chromatin. Nat. Rev 14, 347–359. 10.1038/nrg3413.

14. Mashtalir N, D'Avino AR, Michel BC, Luo J, Pan J, Otto JE, Zullow HJ, McKenzie ZM, Kubiak RL, St. Pierre R, et al. (2018). Modular Organization and Assembly of SWI/SNF Family Chromatin Remodeling Complexes. Cell 175, 1272–1288.e20. 10.1016/j.cell.2018.09.032. [PubMed: 30343899]

15. Ho L, and Crabtree GR (2010). Chromatin remodelling during development. Nature 463, 474–484. 10.1038/nature08911. [PubMed: 20110991]

16. Yoo AS, Staahl BT, Chen L, and Crabtree GR (2009). MicroRNA-mediated switching of chromatin-remodelling complexes in neural development. Nature 460, 642–646. 10.1038/nature08139. [PubMed: 19561591]

17. Yoo AS, Sun AX, Li L, Shcheglovitov A, Portmann T, Li Y, Lee-Messer C, Dolmetsch RE, Tsien RW, and Crabtree GR (2011). MicroRNA-mediated conversion of human fibroblasts to neurons. Nature 476, 228–231. 10.1038/nature10323. [PubMed: 21753754]

18. Wu JI, Lessard J, Olave IA, Qiu Z, Ghosh A, Graef IA, and Crabtree GR (2007). Regulation of dendritic development by neuron-specific chromatin remodeling complexes. Neuron 56, 94–108. S0896-6273(07)00664-2 [pii]. [PubMed: 17920018]

19. Vogel-Ciernia A, Matheos DP, Barrett RM, Kramár EA, Azzawi S, Chen Y, Magnan CN, Zeller M, Sylvain A, Haettig J, et al. (2013). The neuron-specific chromatin regulatory subunit BAF53b is necessary for synaptic plasticity and memory. Nat. Neurosci 16, 552–561. 10.1038/nn.3359. [PubMed: 23525042]

20. Tuoc TC, Boretius S, Sansom SN, Pitulescu ME, Frahm J, Live-sey FJ, and Stoykova A (2013). Chromatin regulation by BAF170 controls cerebral cortical size and thickness. Dev. Cell 25, 256–269. 10.1016/j.devcel.2013.04.005. [PubMed: 23643363]

21. Matsumoto S, Banine F, Struve J, Xing R, Adams C, Liu Y, Metzger D, Chambon P, Rao MS, and Sherman LS (2006). Brg1 is required for murine neural stem cell maintenance and gliogenesis. Dev. Biol 289, 372–383. S0012-1606(05)00770-0 [pii]. [PubMed: 16330018]

22. Reyes JC, Barra J, Muchardt C, Camus A, Babinet C, and Yaniv M (1998). Altered control of cellular proliferation in the absence of mammalian brahma (SNF2alpha). EMBO J. 17, 6979–6991. 10.1093/emboj/17.23.6979. [PubMed: 9843504]

23. Hoyer J, Ekici AB, Endele S, Popp B, Zweier C, Wiesener A, Wohlleber E, Dufke A, Rossier E, Petsch C, et al. (2012). Haploinsufficiency of ARID1B, a member of the SWI/SNF-a chromatin-remodeling complex, is a frequent cause of intellectual disability. Am. J. Hum. Genet 90, 565–572. 10.1016/j.ajhg.2012.02.007. [PubMed: 22405089]

24. Halgren C, Kjaergaard S, Bak M, Hansen C, El-Schich Z, Anderson CM, Henriksen KF, Hjalgrim H, Kirchhoff M, Bijlsma EK, et al. (2012). Corpus callosum abnormalities, intellectual disability,

speech impairment, and autism in patients with haploinsufficiency of ARID1B. Clin. Genet 82, 248–255. 10.1111/j.1399-0004.2011.01755.x. [PubMed: 21801163]

25. Deciphering Developmental Disorders Study (2015). Large-scale discovery of novel genetic causes of developmental disorders. Nature 519, 223–228. 10.1038/nature14135. [PubMed: 25533962]
26. Santen GWE, Aten E, Sun Y, Almomani R, Gilissen C, Nielsen M, Kant SG, Snoeck IN, Peeters EAJ, Hilhorst-Hofstee Y, et al. (2012). Mutations in SWI/SNF chromatin remodeling complex gene ARID1B cause Coffin-Siris syndrome. Nat. Genet 44, 379–380. 10.1038/ng.2217. [PubMed: 22426309]
27. Zhang Z, Cao M, Chang CW, Wang C, Shi X, Zhan X, Birnbaum SG, Bezprozvanny I, Huber KM, and Wu JI (2016). Autism-Associated Chromatin Regulator Brg1/SmarcA4 Is Required for Synapse Development and Myocyte Enhancer Factor 2-Mediated Synapse Remodeling. Mol. Cell Biol 36, 70–83. 10.1128/MCB.00534-15. [PubMed: 26459759]
28. Valencia AM, Sankar A, van der Sluijs PJ, Satterstrom FK, Fu J, Talkowski ME, Vergano SAS, Santen GWE, and Kadoch C (2023). Landscape of mSWI/SNF chromatin remodeling complex perturbations in neurodevelopmental disorders. Nat. Genet 55, 1400–1412. 10.1038/s41588-023-01451-6. [PubMed: 37500730]
29. Alfert A, Moreno N, and Kerl K (2019). The BAF complex in development and disease. Epigenet. Chromatin 12, 19. 10.1186/s13072-019-0264-y.
30. Peterson CL, and Herskowitz I (1992). Characterization of the yeast SWI1, SWI2, and SWI3 genes, which encode a global activator of transcription. Cell 68, 573–583. 10.1016/0092-8674(92)90192-F. [PubMed: 1339306]
31. Hirschhorn JN, Brown SA, Clark CD, and Winston F (1992). Evidence that SNF2/SWI2 and SNF5 activate transcription in yeast by altering chromatin structure. Genes Dev. 6, 2288–2298. 10.1101/gad.6.12a.2288. [PubMed: 1459453]
32. Paun O, Tan YX, Patel H, Strohbuecker S, Ghanate A, Cobolli-Gigli C, Llorian Sopena M, Gerontogianni L, Goldstone R, Ang S-L, et al. (2023). Pioneer factor ASCL1 cooperates with the mSWI/SNF complex at distal regulatory elements to regulate human neural differentiation. Genes Dev. 37, 218–242. 10.1101/gad.350269.122. [PubMed: 36931659]
33. Alver BH, Kim KH, Lu P, Wang X, Manchester HE, Wang W, Haswell JR, Park PJ, and Roberts CWM (2017). The SWI/SNF chromatin remodelling complex is required for maintenance of lineage specific enhancers. Nat. Commun 8, 14648. 10.1038/ncomms14648. [PubMed: 28262751]
34. Mathur R, Alver BH, San Roman AK, Wilson BG, Wang X, Agoston AT, Park PJ, Shivdasani RA, and Roberts CWM (2017). ARID1A loss impairs enhancer-mediated gene regulation and drives colon cancer in mice. Nat. Genet 49, 296–302. 10.1038/ng.3744. [PubMed: 27941798]
35. Nakayama RT, Pulice JL, Valencia AM, McBride MJ, McKenzie ZM, Gillespie MA, Ku WL, Teng M, Cui K, Williams RT, et al. (2017). SMARCB1 is required for widespread BAF complex–mediated activation of enhancers and bivalent promoters. Nat. Genet 49, 1613–1623. 10.1038/ng.3958. [PubMed: 28945250]
36. Park Y-K, Lee J-E, Yan Z, McKernan K, O'Haren T, Wang W, Peng W, and Ge K (2021). Interplay of BAF and MLL4 promotes cell type-specific enhancer activation. Nat. Commun 12, 1630. 10.1038/s41467-021-21893-y. [PubMed: 33712604]
37. Brahma S, and Henikoff S (2024). The BAF chromatin remodeler synergizes with RNA polymerase II and transcription factors to evict nucleosomes. Nat. Genet 56, 100–111. 10.1038/s41588-023-01603-8. [PubMed: 38049663]
38. Oruba A, Saccani S, and van Essen D (2020). Role of cell-type specific nucleosome positioning in inducible activation of mammalian promoters. Nat. Commun 11, 1075. 10.1038/s41467-020-14950-5. [PubMed: 32103026]
39. Fujinaga K, Huang F, and Peterlin BM (2023). P-TEFb: The master regulator of transcription elongation. Mol. Cell 83, 393–403. 10.1016/j.molcel.2022.12.006. [PubMed: 36599353]
40. Cramer P (2019). Eukaryotic Transcription Turns 50. Cell 179, 808–812. 10.1016/j.cell.2019.09.018. [PubMed: 31675494]
41. Mohamed AA, Vazquez Nunez R, and Vos SM (2022). Structural advances in transcription elongation. Curr. Opin. Struct. Biol 75, 102422. 10.1016/j.sbi.2022.102422. [PubMed: 35816930]

42. Vos SM, Farnung L, Linden A, Urlaub H, and Cramer P (2020). Structure of complete Pol II–DSIF–PAF–SPT6 transcription complex reveals RTF1 allosteric activation. Nat. Struct. Mol. Biol 27, 668–677. 10.1038/s41594-020-0437-1. [PubMed: 32541898]
43. Kulaeva OI, Hsieh F-K, and Studitsky VM (2010). RNA polymerase complexes cooperate to relieve the nucleosomal barrier and evict his-tones. Proc. Natl. Acad. Sci 107, 11325–11330. 10.1073/pnas.1001148107. [PubMed: 20534568]
44. Schwabish MA, and Struhl K (2007). The Swi/Snf Complex Is Important for Histone Eviction during Transcriptional Activation and RNA Polymerase II Elongation In Vivo. Mol. Cell Biol 27, 6987–6995. 10.1128/MCB.00717-07. [PubMed: 17709398]
45. Subtil-Rodríguez A, and Reyes JC (2010). BRG1 helps RNA polymerase II to overcome a nucleosomal barrier during elongation, in vivo. EMBO Rep. 11, 751–757. 10.1038/embor.2010.131. [PubMed: 20829883]
46. Armstrong JA, Papoulas O, Daubresse G, Sperling AS, Lis JT, Scott MP, and Tamkun JW (2002). The Drosophila BRM complex facilitates global transcription by RNA polymerase II. EMBO J. 21, 5245–5254. 10.1093/emboj/cdf517. [PubMed: 12356740]
47. Batsché E, Yaniv M, and Muchardt C (2006). The human SWI/SNF subunit Brm is a regulator of alternative splicing. Nat. Struct. Mol. Biol 13, 22–29. 10.1038/nsmb1030. [PubMed: 16341228]
48. Corey LL, Weirich CS, Benjamin IJ, and Kingston RE (2003). Localized recruitment of a chromatin-remodeling activity by an activator in vivo drives transcriptional elongation. Genes Dev. 17, 1392–1401. 10.1101/gad.1071803. [PubMed: 12782657]
49. Mazina MY, Nikolenko YV, Krasnov AN, and Vorobyeva NE (2016). SWI/SNF protein complexes participate in the initiation and elongation stages of Drosophila hsp70 gene transcription. Russ. J. Genet 52, 141–145. 10.1134/S1022795416010105.
50. Tyssowski KM, DeStefino NR, Cho J-H, Dunn CJ, Poston RG, Carty CE, Jones RD, Chang SM, Romeo P, Wurzelmann MK, et al. (2018). Different Neuronal Activity Patterns Induce Different Gene Expression Programs. Neuron 98, 530–546.e11. 10.1016/j.neuron.2018.04.001. [PubMed: 29681534]
51. Saha RN, Wissink EM, Bailey ER, Zhao M, Fargo DC, Hwang J-Y, Daigle KR, Fenn JD, Adelman K, and Dudek SM (2011). Rapid activity-induced transcription of Arc and other IEGs relies on poised RNA polymerase II. Nat. Neurosci 14, 848–856. 10.1038/nn.2839. [PubMed: 21623364]
52. Fujita T, Ryser S, Piuz I, and Schlegel W (2008). Up-Regulation of P-TEFb by the MEK1-Extracellular Signal-Regulated Kinase Signaling Pathway Contributes to Stimulated Transcription Elongation of Immediate Early Genes in Neuroendocrine Cells. Mol. Cell Biol 28, 1630–1643. 10.1128/MCB.01767-07. [PubMed: 18086894]
53. Farnaby W, Koegl M, Roy MJ, Whitworth C, Diers E, Trainor N, Zollman D, Steurer S, Karolyi-Oezguer J, Riedmueller C, et al. (2019). BAF complex vulnerabilities in cancer demonstrated via structure-based PROTAC design. Nat. Chem. Biol 15, 672–680. 10.1038/s41589-019-0294-6. [PubMed: 31178587]
54. Dunn CJ, Sarkar P, Bailey ER, Farris S, Zhao M, Ward JM, Dudek SM, and Saha RN (2017). Histone hypervariants H2A.Z.1 and H2A.Z.2 play independent and context-specific roles in neuronal activity-induced transcription of Arc/Arg3.1 and other immediate early genes. eNeuro 4, 1–30. 10.1523/ENEURO.0040-17.2017.
55. Rienecker KDA, Poston RG, Segales JS, Finholm IW, Sono MH, Munteanu SJ, Ghaninejad-Esfahani M, Rejepova A, Tejeda-Garibay S, Wickman K, et al. (2022). Mild membrane depolarization in neurons induces immediate early gene transcription and acutely subdues responses to successive stimulus. J. Biol. Chem 298, 102278. 10.1016/J.JBC.2022.102278. [PubMed: 35863435]
56. Papillon JPN, Nakajima K, Adair CD, Hempel J, Jouk AO, Karki RG, Mathieu S, Möbitz H, Ntaganda R, Smith T, et al. (2018). Discovery of Orally Active Inhibitors of Brahma Homolog (BRM)/SMARCA2 ATPase Activity for the Treatment of Brahma Related Gene 1 (BRG1)/SMARCA4-Mutant Cancers. J. Med. Chem 61, 10155–10172. 10.1021/acs.jmedchem.8b01318. [PubMed: 30339381]
57. Battistello E, Hixon KA, Comstock DE, Collings CK, Chen X, Rodriguez Hernaez J, Lee S, Cervantes KS, Hinkley MM, Ntatsoulis K, et al. (2023). Stepwise activities of mSWI/SNF family

chromatin remodeling complexes direct T cell activation and exhaustion. Mol. Cell 83, 1216–1236.e12. 10.1016/j.molcel.2023.02.026. [PubMed: 36944333]

58. Poston RG, Dunn CJ, Sarkar P, and Saha RN (2018). Persistent 6-OH-BDE-47 exposure impairs functional neuronal maturation and alters expression of neurodevelopmentally-relevant chromatin remodelers. Environ. Epigenet 4, dvx020. 10.1093/eep/dvx020.
59. Marian CA, Stoszko M, Wang L, Leighty MW, de Crignis E, Maschinot CA, Gatchalian J, Carter BC, Chowdhury B, Hargreaves DC, et al. (2018). Small Molecule Targeting of Specific BAF (mSWI/SNF) Complexes for HIV Latency Reversal. Cell Chem. Biol 25, 1443–1455.e14. 10.1016/j.chembiol.2018.08.004. [PubMed: 30197195]
60. Jafari R, Almqvist H, Axelsson H, Ignatushchenko M, Lundbäck T, Nordlund P, and Martinez Molina D (2014). The cellular thermal shift assay for evaluating drug target interactions in cells. Nat. Protoc 9, 2100–2122. 10.1038/nprot.2014.138. [PubMed: 25101824]
61. Ordonez-Rubiano SC, Maschinot CA, Wang S, Sood S, Baracaldo-Lancheros LF, Strohmier BP, McQuade AJ, Smith BC, and Dykhuizen EC (2023). Rational Design and Development of Selective BRD7 Bromodomain Inhibitors and Their Activity in Prostate Cancer. J. Med. Chem 66, 11250–11270. 10.1021/acs.jmedchem.3c00671. [PubMed: 37552884]
62. Theodoulou NH, Bamborough P, Bannister AJ, Becher I, Bit RA, Che KH, Chung C.w., Dittmann A, Drewes G, Drewry DH, et al. (2016). Discovery of I-BRD9, a Selective Cell Active Chemical Probe for Bromodomain Containing Protein 9 Inhibition. J. Med. Chem 59, 1425–1439. 10.1021/acs.jmedchem.5b00256. [PubMed: 25856009]
63. Zoppi V, Hughes SJ, Maniaci C, Testa A, Gmaschitz T, Wieshofer C, Koegl M, Riching KM, Daniels DL, Spallarossa A, and Ciulli A (2019). Iterative Design and Optimization of Initially Inactive Proteolysis Targeting Chimeras (PROTACs) Identify VZ185 as a Potent, Fast, and Selective von Hippel-Lindau (VHL) Based Dual Degrader Probe of BRD9 and BRD7. J. Med. Chem 62, 699–726. 10.1021/acs.jmedchem.8b01413. [PubMed: 30540463]
64. Patil A, Strom AR, Paulo JA, Collings CK, Ruff KM, Shinn MK, Sankar A, Cervantes KS, Wauer T, St. Laurent JD, et al. (2023). A disordered region controls cBAF activity via condensation and partner recruitment. Cell 186, 4936–4955.e26. 10.1016/j.cell.2023.08.032. [PubMed: 37788668]
65. Dignam JD, Lebovitz RM, and Roeder RG (1983). Accurate transcription initiation by RNA polymerase II in a soluble extract from isolated mammalian nuclei. Nucleic Acids Res. 11, 1475–1489. 10.1093/nar/11.5.1475. [PubMed: 6828386]
66. Mayer A, and Churchman LS (2016). Genome-wide profiling of RNA polymerase transcription at nucleotide resolution in human cells with native elongating transcript sequencing. Nat. Protoc 11, 813–833. 10.1038/nprot.2016.047. [PubMed: 27010758]
67. Martell DJ, Merens HE, Caulier A, Fiorini C, Ulirsch JC, Ietswaart R, Choquet K, Graziadei G, Brancaleoni V, Cappellini MD, et al. (2023). RNA polymerase II pausing temporally coordinates cell cycle progression and erythroid differentiation. Dev. Cell 58, 2112–2127.e4. 10.1016/j.devcel.2023.07.018. [PubMed: 37586368]
68. Nechaev S, and Adelman K (2008). Promoter-proximal Pol II: When stalling speeds things up. Cell Cycle 7, 1539–1544. 10.4161/cc.7.11.6006. [PubMed: 18469524]
69. Aoi Y, Takahashi YH, Shah AP, Iwanaszko M, Rendleman EJ, Khan NH, Cho B-K, Goo YA, Ganesan S, Kelleher NL, and Shilatifard A (2021). SPT5 stabilization of promoter-proximal RNA polymerase II. Mol. Cell 81, 4413–4424.e5. 10.1016/j.molcel.2021.08.006. [PubMed: 34480849]
70. Madabhushi R, and Kim T-K (2018). Emerging themes in neuronal activity-dependent gene expression. Mol. Cell. Neurosci 87, 27–34. 10.1016/j.mcn.2017.11.009. [PubMed: 29254824]
71. Peterlin BM, and Price DH (2006). Controlling the Elongation Phase of Transcription with P-TEFb. Mol. Cell 23, 297–305. 10.1016/j.molcel.2006.06.014. [PubMed: 16885020]
72. Vos SM, Farnung L, Boehning M, Wigge C, Linden A, Urlaub H, and Cramer P (2018). Structure of activated transcription complex Pol II–DSIF–PAF–SPT6. Nature 560, 607–612. 10.1038/s41586-018-0440-4. [PubMed: 30135578]
73. Zhang H, Pandey S, Travers M, Sun H, Morton G, Madzo J, Chung W, Khowsathit J, Perez-Leal O, Barrero CA, et al. (2018). Targeting CDK9 Reactivates Epigenetically Silenced Genes in Cancer. Cell 175, 1244–1258.e26. 10.1016/j.cell.2018.09.051. [PubMed: 30454645]

74. Olson CM, Jiang B, Erb MA, Liang Y, Doctor ZM, Zhang Z, Zhang T, Kwiatkowski N, Boukhali M, Green JL, et al. (2018). Pharmacological perturbation of CDK9 using selective CDK9 inhibition or degradation. Nat. Chem. Biol 14, 163–170. 10.1038/nchembio.2538. [PubMed: 29251720]
75. Jonkers I, Kwak H, and Lis JT (2014). Genome-wide dynamics of Pol II elongation and its interplay with promoter proximal pausing, chromatin, and exons. Elife 3, e02407. 10.7554/eLife.02407. [PubMed: 24843027]
76. Aoi Y, and Shilatifard A (2023). Transcriptional elongation control in developmental gene expression, aging, and disease. Mol. Cell 83, 3972–3999. 10.1016/j.molcel.2023.10.004. [PubMed: 37922911]
77. Dunn CJ, Sarkar P, Bailey ER, Farris S, Zhao M, Ward JM, Dudek SM, and Saha RN (2017). Histone Hypervariants H2A.Z.1 and H2A.Z.2 Play Independent and Context-Specific Roles in Neuronal Activity-Induced Transcription of Arc/Arg3.1 and Other Immediate Early Genes. eNeuro 4, ENEURO.0040-17.2017. 10.1523/ENEURO.0040-17.2017.
78. Che Z, Liu X, Dai Q, Fang K, Guo C, Yue J, Fang H, Xie P, Luo Z, and Lin C (2024). Distinct roles of two SEC scaffold proteins, AFF1 and AFF4, in regulating RNA polymerase II transcription elongation. J. Mol. Cell Biol 15, mjad049. 10.1093/jmcb/mjad049.
79. Chen F, Gao X, and Shilatifard A (2015). Stably paused genes revealed through inhibition of transcription initiation by the TFIIH inhibitor triptolide. Genes Dev. 29, 39–47. 10.1101/gad.246173.114. [PubMed: 25561494]
80. Elrod ND, Henriques T, Huang K-L, Tatomer DC, Wilusz JE, Wagner EJ, and Adelman K (2019). The Integrator Complex Attenuates Promoter-Proximal Transcription at Protein-Coding Genes. Mol. Cell 76, 738–752.e7. 10.1016/j.molcel.2019.10.034. [PubMed: 31809743]
81. Gourisankar S, Wenderski W, Paulo JA, Kim SH, Roepke K, Ellis C, Gygi SP, and Crabtree GR (2023). Synaptic Activity Causes Minute-scale Changes in BAF Complex Composition and Function. Preprint at: bioRxiv. 10.1101/2023.10.13.562244
82. Iurlaro M, Stadler MB, Masoni F, Jagani Z, Galli GG, and Schubeler D (2021). Mammalian SWI/SNF continuously restores local accessibility to chromatin. Nat. Genet 53, 279–287. 10.1038/s41588-020-00768-w. [PubMed: 33558757]
83. Hoffman JA, Trotter KW, Ward JM, and Archer TK (2018). BRG1 governs glucocorticoid receptor interactions with chromatin and pioneer factors across the genome. Elife 7, e35073. 10.7554/eLife.35073. [PubMed: 29792595]
84. Kim B, Luo Y, Zhan X, Zhang Z, Shi X, Yi J, Xuan Z, and Wu J (2021). Neuronal activity-induced BRG1 phosphorylation regulates enhancer activation. Cell Rep. 36, 109357. 10.1016/j.celrep.2021.109357. [PubMed: 34260936]
85. Zhang X, Li B, Li W, Ma L, Zheng D, Li L, Yang W, Chu M, Chen W, Mailman RB, et al. (2014). Transcriptional Repression by the BRG1-SWI/SNF Complex Affects the Pluripotency of Human Embryonic Stem Cells. Stem Cell Rep. 3, 460–474. 10.1016/j.stemcr.2014.07.004.
86. Tolstorukov MY, Sansam CG, Lu P, Koellhoffer EC, Helming KC, Alver BH, Tillman EJ, Evans JA, Wilson BG, Park PJ, and Roberts CWM (2013). Swi/Snf chromatin remodeling/tumor suppressor complex establishes nucleosome occupancy at target promoters. Proc. Natl. Acad. Sci 110, 10165–10170. 10.1073/pnas.1302209110. [PubMed: 23723349]
87. Trizzino M, Barbieri E, Petracovici A, Wu S, Welsh SA, Owens TA, Licciulli S, Zhang R, and Gardini A (2018). The Tumor Suppressor ARID1A Controls Global Transcription via Pausing of RNA Polymerase II. Cell Rep. 23, 3933–3945. 10.1016/j.celrep.2018.05.097. [PubMed: 29949775]
88. Mayer A, di Iulio J, Maleri S, Eser U, Vierstra J, Reynolds A, Sand-strom R, Stamatoyannopoulos JA, and Churchman LS (2015). Native Elongating Transcript Sequencing Reveals Human Transcriptional Activity at Nucleotide Resolution. Cell 161, 541–554. 10.1016/j.cell.2015.03.010. [PubMed: 25910208]
89. Wenderski W, Wang L, Krokhotin A, Walsh JJ, Li H, Shoji H, Ghosh S, George RD, Miller EL, Elias L, et al. (2020). Loss of the neural-specific BAF subunit ACTL6B relieves repression of early response genes and causes recessive autism. Proc. Natl. Acad. Sci. USA 117, 10055–10066. 10.1073/pnas.1908238117. [PubMed: 32312822]

90. Modur V, Singh N, Mohanty V, Chung E, Muhammad B, Choi K, Chen X, Chetal K, Ratner N, Salomonis N, et al. (2018). Defective transcription elongation in a subset of cancers confers immunotherapy resistance. Nat. Commun 9, 4410. 10.1038/s41467-018-06810-0. [PubMed: 30353012]

91. Miller TE, Liau BB, Wallace LC, Morton AR, Xie Q, Dixit D, Factor DC, Kim LJY, Morrow JJ, Wu Q, et al. (2017). Transcription elongation factors represent in vivo cancer dependencies in glioblastoma. Nature 547, 355–359. 10.1038/nature23000. [PubMed: 28678782]

92. Muhammad B, Parks LG, Komurov K, and Privette Vinnedge LM (2022). Defective transcription elongation in human cancers imposes targetable proteotoxic vulnerability. Transl. Oncol 16, 101323. 10.1016/j.tranon.2021.101323. [PubMed: 34954455]

93. St. Pierre R, and Kadoch C (2017). Mammalian SWI/SNF complexes in cancer: emerging therapeutic opportunities. Curr. Opin. Genet. Dev 42, 56–67. 10.1016/j.gde.2017.02.004. [PubMed: 28391084]

94. King IF, Yandava CN, Mabb AM, Hsiao JS, Huang HS, Pearson BL, Calabrese JM, Starmer J, Parker JS, Magnuson T, et al. (2013). Topoisomerases facilitate transcription of long genes linked to autism. Nature 501, 58–62. 10.1038/nature12504. [PubMed: 23995680]

95. Qiu Z, Zhao L, Shen JZ, Liang Z, Wu Q, Yang K, Min L, Gimple RC, Yang Q, Bhargava S, et al. (2022). Transcription Elongation Machinery Is a Druggable Dependency and Potentiates Immunotherapy in Glioblastoma Stem Cells. Cancer Discov. 12, 502–521. 10.1158/2159-8290.CD-20-1848. [PubMed: 34615656]

96. Bidart M, El Atifi M, Miladi S, Rendu J, Satre V, Ray PF, Bosson C, Devillard F, Lehalle D, Malan V, et al. (2017). Microduplication of the ARID1A gene causes intellectual disability with recognizable syndromic features. Genet. Med 19, 701–710. 10.1038/gim.2016.180. [PubMed: 27906199]

97. Machol K, Rousseau J, Ehresmann S, Garcia T, Nguyen TTM, Spillmann RC, Sullivan JA, Shashi V, Jiang YH, Stong N, et al. (2019). Expanding the Spectrum of BAF-Related Disorders: De Novo Variants in SMARCC2 Cause a Syndrome with Intellectual Disability and Developmental Delay. Am. J. Hum. Genet 104, 164–178. 10.1016/j.ajhg.2018.11.007. [PubMed: 30580808]

98. Neale BM, Kou Y, Liu L, Ma'ayan A, Samocha KE, Sabo A, Lin CF, Stevens C, Wang LS, Makarov V, et al. (2012). Patterns and rates of exonic de novo mutations in autism spectrum disorders. Nature 485, 242–245. 10.1038/nature11011. [PubMed: 22495311]

99. Iossifov I, Levy D, Allen J, Ye K, Ronemus M, Lee YH, Yamrom B, and Wigler M (2015). Low load for disruptive mutations in autism genes and their biased transmission. Proc. Natl. Acad. Sci. USA 112, E5600–E5607. 10.1073/pnas.1516376112. [PubMed: 26401017]

100. Takata A, Ionita-Laza I, Gogos JA, Xu B, and Karayiorgou M (2016). De Novo Synonymous Mutations in Regulatory Elements Contribute to the Genetic Etiology of Autism and Schizophrenia. Neuron 89, 940–947. 10.1016/j.neuron.2016.02.024. [PubMed: 26938441]

101. Bosch E, Popp B, Güse E, Skinner C, van der Sluijs PJ, Maystadt I, Pinto AM, Renieri A, Bruno LP, Granata S, et al. (2023). Elucidating the clinical and molecular spectrum of SMARCC2-associated NDD in a cohort of 65 affected individuals. Genet. Med 25, 100950. 10.1016/j.gim.2023.100950. [PubMed: 37551667]

102. Navickas SM, Giles KA, Brettingham-Moore KH, and Taberlay PC (2023). The role of chromatin remodeler SMARCA4/BRG1 in brain cancers: a potential therapeutic target. Oncogene 42, 2363–2373. 10.1038/s41388-023-02773-9. [PubMed: 37433987]

Highlights

- The neuronal BAF complex mediates activity-induced immediate early gene transcription
- Neuronal activity induces extrabasal assembly of the nBAF complex
- Neuronal BAF interacts with the RNA Pol II elongation complex and mediates productive elongation
- ATPase activity is required for mediation of RNA Pol II elongation by the BAF complex

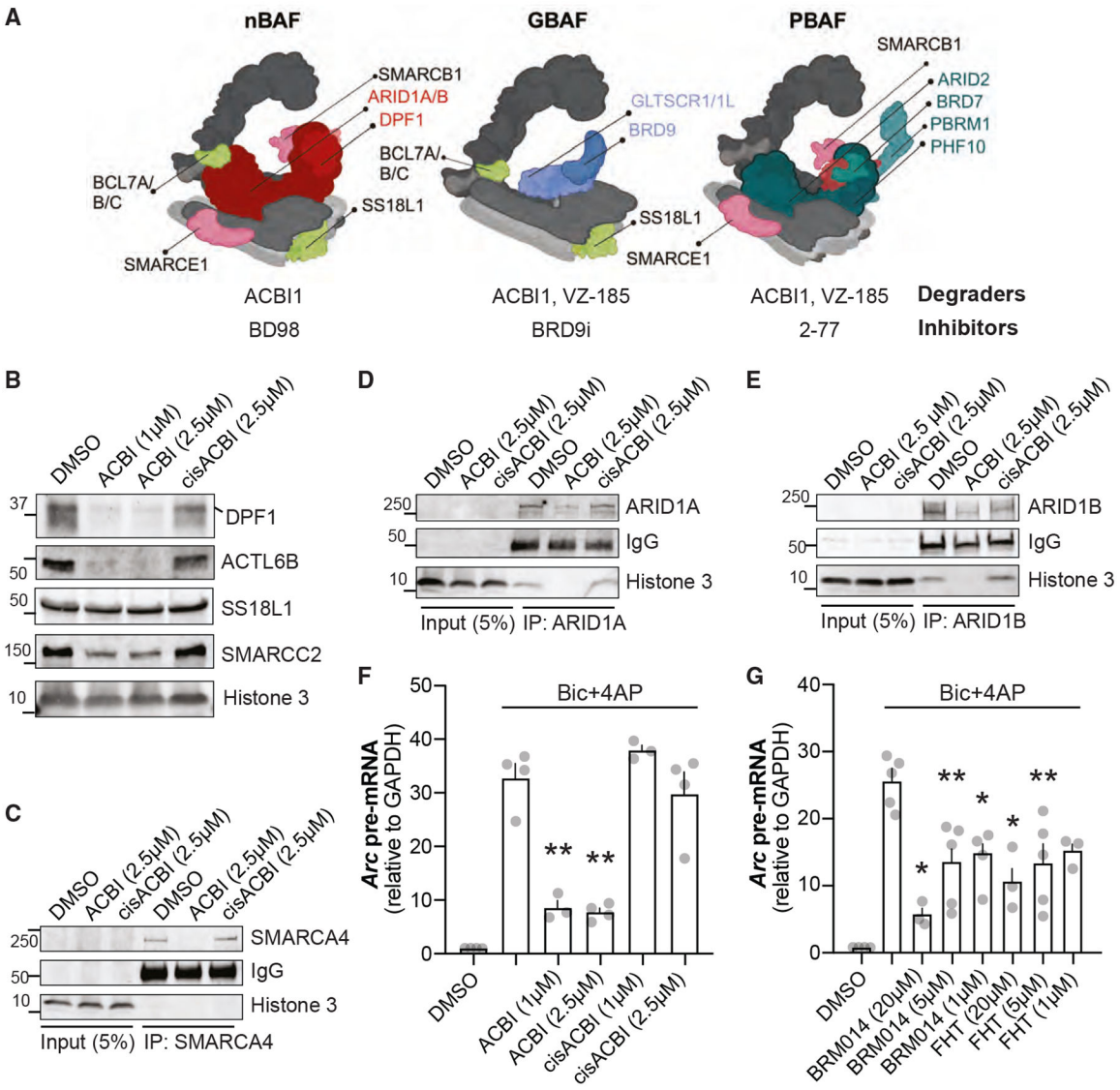

Figure 1. BAF complex is required for optimal Arc transcription

(A) Schematic representation of three biochemically distinct BAF complexes: nBAF (neuronal cBAF), GBAF, and PBAF. Complex-defining unique subunits are represented in colors. Subunits shared by all three complexes are not indicated. Degraders and small-molecule inhibitors to target each complex are noted below. Schematic was created using BioRender.

(B) Neurons were treated with DMSO (control) or the indicated concentrations of ACBI1 or *cis*-ACBI1 (inactive isomer of ACBI1) for 3 h. Whole-cell lysates were electrophoresed, western blotted, and probed for the indicated BAF subunits.

(C–E) Neuronal lysates were used to immunoprecipitate SMARCA4 (C), ARID1A (D), and ARID1B (E). Five percent of the cell lysate was used as input. Histone 3 and IgG are depicted as loading controls.

(F and G) Transcriptional assays in which *Arc* pre-mRNA normalized by GAPDH pre-mRNA levels is illustrated. (F) Neurons were treated with ACBI1 or *cis*-ACBI1 for 3 h

followed by bicuculline and 4AP treatment for 15 min (Bic + 4AP). (G) Neurons were treated with BAF ATPase domain inhibitors BRM014 and FHT for 30 min, followed by Bic + 4AP treatment to induce neuronal activity. Gray dots represent biological replicates, error bars show SE of the mean. *$p < 0.05$ and **$p < 0.01$. One-way ANOVA was followed by Tukey's *post hoc* test. Approximate position of the nearest molecular weight marker is depicted against each band.

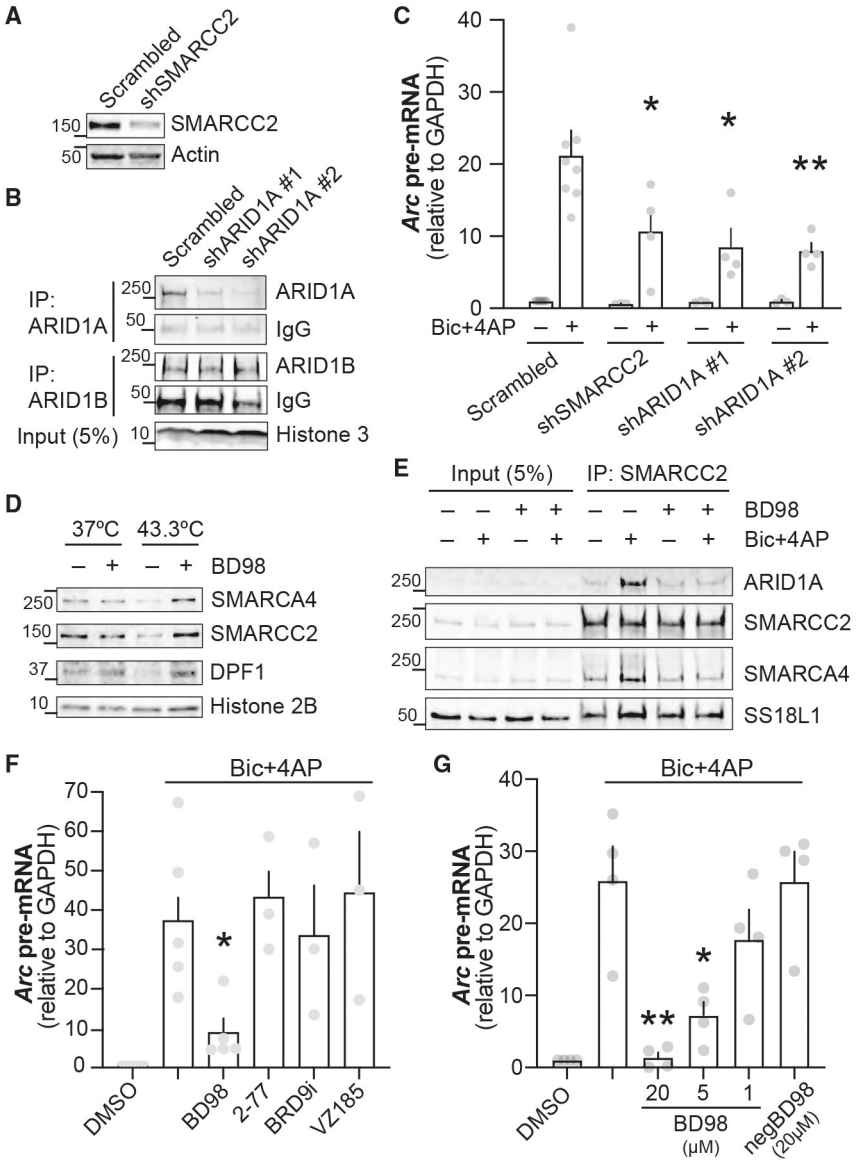

Figure 2. RNAi-dependent depletion and pharmacological perturbation of nBAF complex subunits attenuate Arc transcription

(A and B) Protein levels indicating knockdown of SMARCC2 and ARID1A. Neurons were infected with lentiviruses to deliver short hairpin RNA (shRNA) targeted against *SMARCC2* (3 days) or *ARID1A* (5 days). Scrambled shRNA was used as control. Knockdown of SMARCC2 (A; whole-cell lysate) and ARID1A (B; immunoprecipitation of whole-cell lysate) was verified by protein levels. Specificity of ARID1A RNAi is depicted by immunoprecipitation of ARID1B, whose levels remained unaffected.

(C) Neurons depleted of the indicated nBAF subunits were treated with bicuculline and 4AP (Bic + 4AP; neuronal activity) for 15 min. Normalized *Arc* pre-mRNA levels are displayed.

(D) Cellular thermal shift assay (CETSA) was performed on live cells treated with BD98 (20 μM) for 30 min. Cell lysates were then analyzed via western blot to assess thermal stability of SMARCC2, SMARCA4, and nBAF-specific DPF1. All three BAF subunits displayed

stability at higher temperature in BD98-treated neurons, indicating direct binding of the inhibitor with the nBAF complex.

(E) CoIP assay was performed in lysates from neurons preincubated with BD98 (5 μM) followed by Bic + 4AP treatment for 15 min. Anti-SMARCC2 immunoprecipitated samples were separated on a gel and blotted for other BAF subunits. Five percent of the cell lysate was used as input.

(F) Neurons were preincubated for 30 min with BD98 (20 μM), BRD7i (5 μM), and BRD9i (0.2 μM) to inhibit nBAF, PBAF, and GBAF, respectively, followed by Bic + 4AP for 15 min. Normalized *Arc* pre-mRNA levels are displayed.

(G) Similar to the assay in (F), except neurons were preincubated with the indicated doses of BD98. Negative BD98 was used as a control. Gray dots represent biological replicates, and error bars show SE of the mean. *$p < 0.05$ and **$p < 0.01$. One-way ANOVA was performed followed by Tukey's *post hoc* test. Approximate position of the nearest molecular weight marker is depicted against each band.

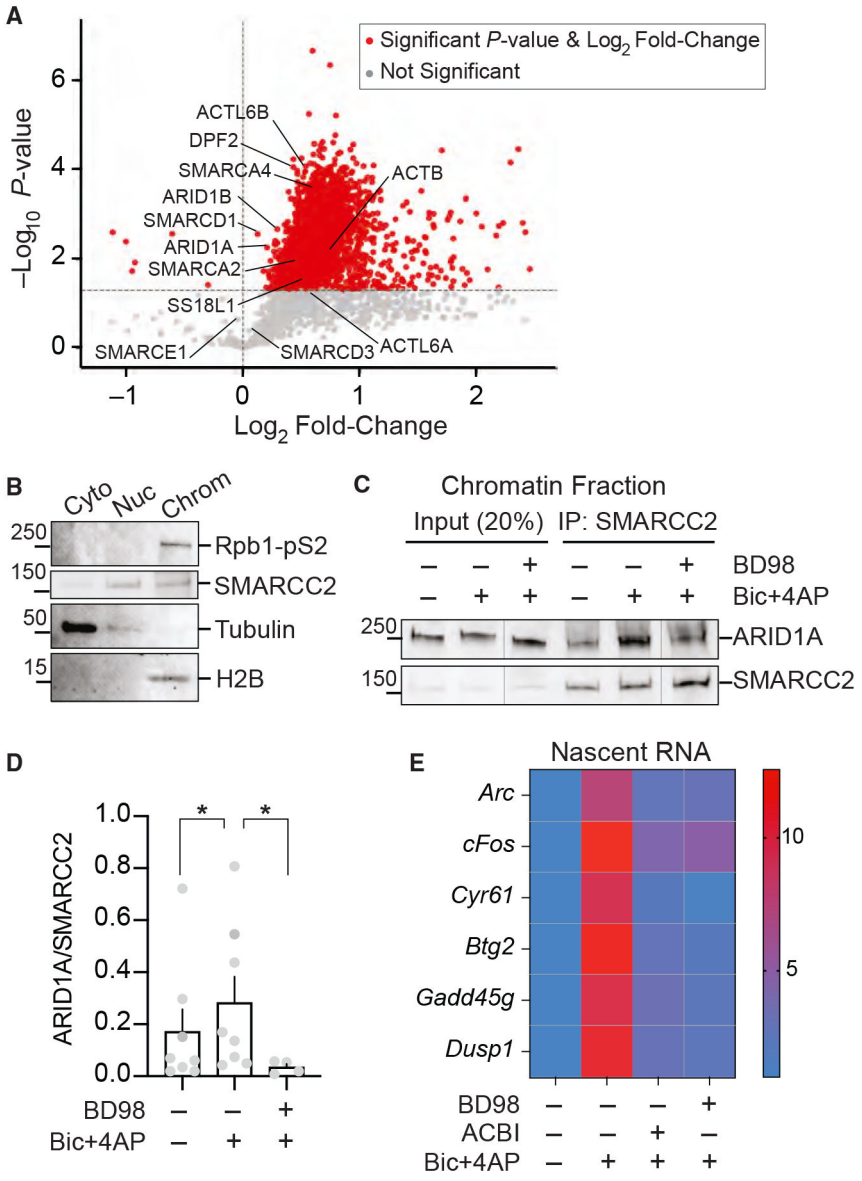

Figure 3. Neuronal activity dynamically assembles nBAF

(A) Immunoprecipitation coupled with mass spectrometry (IP-MS) to investigate changes in the interaction between nBAF subunits in neurons before and after neuronal activity. Cell lysates were immunoprecipitated using an anti-SMARCC2 antibody. Bicuculline treatment and control samples were processed for liquid chromatography-tandem mass spectrometry (LC-MS/MS) analysis. Student's t test was performed, and the difference in $\log_2$ fold change on averages was calculated. *p* values and $\log_2$ fold change (difference) were used to create a volcano plot. $p < 0.05$ and difference thresholds >0.0 and <0.0 (fold change = 2^difference) were used.

(B) Neurons were fractionated into cellular compartments (cytoplasm, nucleoplasm, and chromatin) to isolate the chromatin-bound proteins. Equal percentages of total cell lysate were analyzed via western blot to assess quality of fractionation.

(C) Chromatin fractionation was used and anti-SMARCC2 immunoprecipitated samples were separated on a gel and blotted for other BAF subunits.
(D) Quantification of (C). Individual band intensity values for ARID1A and SMARCC2 were obtained from Image Lab Bio-Rad software. Interaction was assessed by plotting the ratio of ARID1A and SMARCC2 in each treatment.
(E) RNA was extracted from the chromatin fraction, and nascent RNAs for indicated genes were assayed. They are displayed as a heatmap (normalized by GAPDH nascent RNA). Values and statistics for individual genes are shown in Figure S3. Gray dots represent biological replicates; error bars show SE of the mean. *$p < 0.05$.

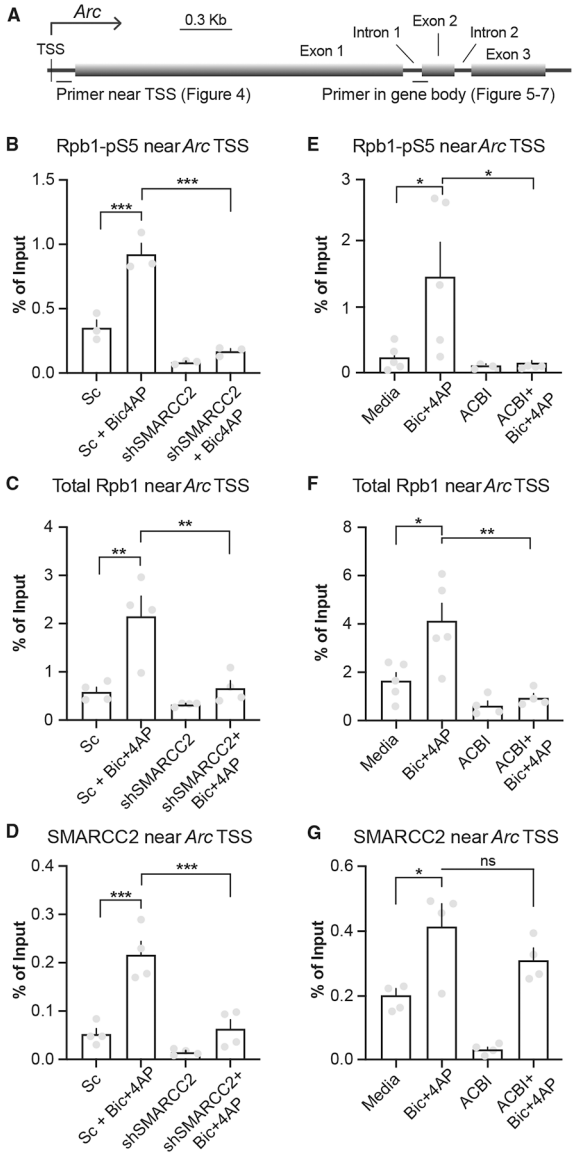

Figure 4. The nBAF complex aids activity-induced RNA Pol II recruitment to the Arc promoter

(A) Schematic representation of *Arc* to show promoter, exons, introns, and primer positions used to quantify immunoprecipitated chromatin in this and other figures. TSS, transcription start site.

(B–G) In (B)–(D), neurons were SMARCC2 depleted by RNAi and knockdown was confirmed by independent western blots (not shown). Sc, scrambled shRNA as control. In (E)–(G), neurons were incubated with ACBI (3 h, 2.5 μM) to degrade SMARCA4. ChIP assays were subsequently performed for all treatments (B)–(G). (B and E) Quantified paused RNA Pol II binding near the *Arc* promoter determined by ChIP with an antibody against Rpb1 phosphorylated at serine 5 in the CTD (Rpb1-pSer5). (C and F) Quantified total RNA Pol II binding near the *Arc* promoter determined by ChIP with antibody against Rpb1-NTD. (D and G) Quantified SMARCC2 binding near the *Arc* promoter determined by ChIP with antibody against SMARCC2. Gray dots represent biological replicates; error bars show SE

of the mean. *$p < 0.05$, **$p < 0.01$, and ***$p < 0.001$. One-way ANOVA followed by Tukey's *post hoc* test was performed.

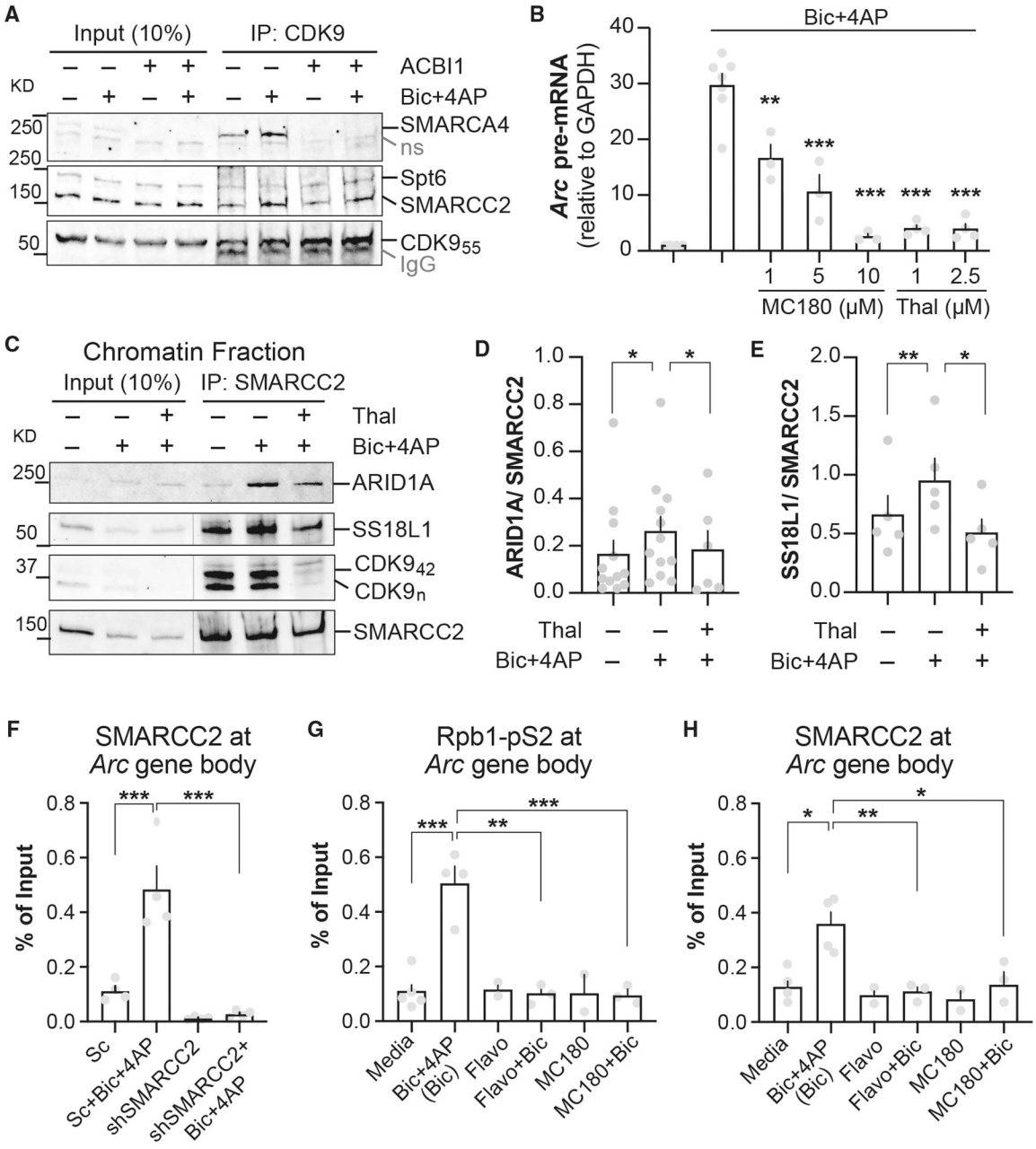

Figure 5. The nBAF complex interacts with and is regulated by RNA Pol II EC

(A) Neurons were incubated for 3 h with ACBI (2.5 μM), and activity was induced by Bic + 4AP for 15 min. CoIP was then performed in neuronal lysates with anti-CDK9. CoIP samples were separated on a gel and blotted for other BAF subunits. SMARCA4 is used as a control to show ACBI efficiency. Spt6 is part of the elongation complex.

(B) Neurons were incubated with MC180 or Thal-SNS-032 for 20 min or 3 h, respectively, followed by activity induction for 15 min with Bic + 4AP. Normalized *Arc* pre-mRNA levels were assayed and are displayed.

(C) Neurons were treated as indicated and fractionated. The chromatin fraction was used, and anti-SMARCC2 coIP samples were electrophoresed and blotted for other BAF subunits.

ARID1A is shown on a blot separate from the others. The ARID1A loading control (SMARCC2) is not displayed here to avoid duplication but is quantified in (D).
(D and E) Quantification of (C) for ARID1A and SS18L1, respectively (normalized by SMARCC2). Quantification was performed as described for Figure 3.
(F) ChIP data to show SMARCC2 binding inside the *Arc* gene body 15 min after stimulation of wild type or neurons depleted of the subunit.
(G) Quantified elongating RNA Pol II binding inside the *Arc* gene body, 15 min after stimulation, determined by ChIP with antibody against Rpb1-pSer2.
(H) Quantified SMARCC2 binding inside the *Arc* gene body, after identical stimulation as in (G), determined by ChIP with antibody against SMARCC2. Gray dots represent biological replicates; error bars show SE of the mean. $*p < 0.05$, $**p < 0.01$, and $***p < 0.001$. One-way ANOVA was performed followed by Tukey's *post hoc* test.

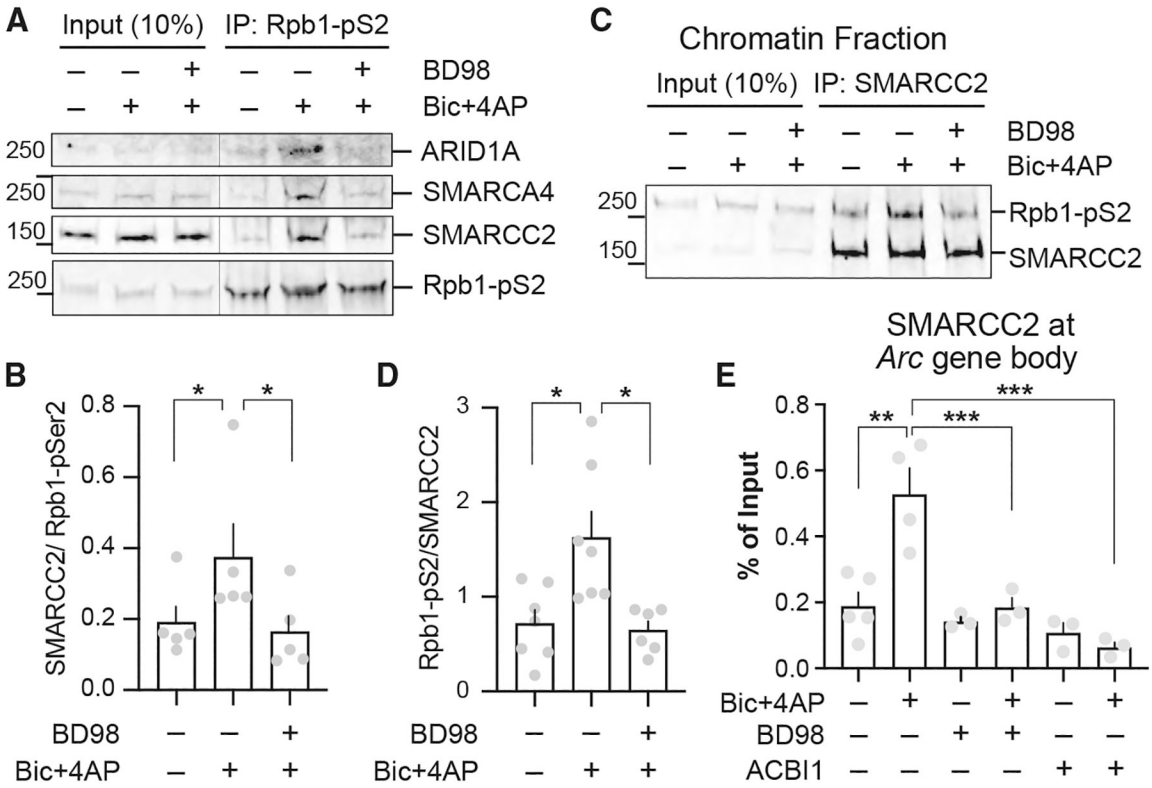

Figure 6. The nBAF complex interacts with elongation-competent RNA Pol II

(A) Neurons were incubated with BD98 (20 min, 5 μM) and activity was induced by Bic + 4AP for 15 min. Interactions between Rpb1-pS2 and the indicated nBAF subunits were assessed using whole-cell lysates.

(B) Quantification of the dataset displayed in (A). Individual band intensities for SMARCC2 and Rpb1-pSer2 were obtained with the ImageLab Bio-Rad software. Interaction was assessed by plotting the ratio of Rpb1-pSer2 and SMARCC2 in each treatment.

(C) Cells were treated as noted and fractionated. The chromatin fraction was used, and anti-SMARCC2 immunoprecipitated samples were electrophoresed and blotted for pSer2-Rpb1.

(D) Quantification of the dataset displayed in (C), performed as in (B).

(E) ChIP data demonstrating SMARCC2 binding inside the *Arc* gene body in response to 15 min of activity in the presence or absence of BD98 or ACBI1. Gray dots represent biological replicates; error bars show SE of the mean. *$p < 0.05$, **$p < 0.01$, and **$p < 0.001$. One-way ANOVA was performed followed by Tukey's *post hoc* test.

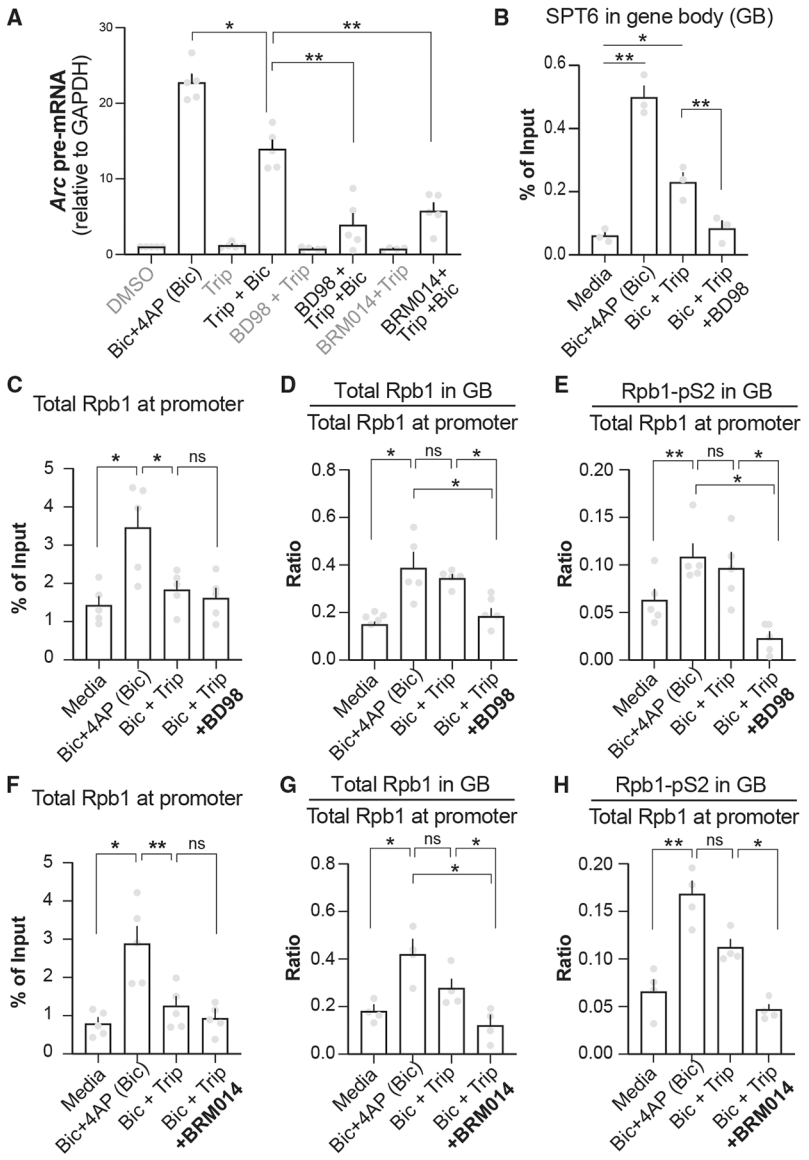

Figure 7. Assembled complex and its ATPase activity are required for RNA Pol II productive elongation

(A) Neurons, as indicated, were incubated with BD98 (5 μM) or BRM014 (5 μM) for 20 and 10 min, respectively, and co-treated with triptolide (1 μM) and Bic + 4AP for 10 min. Activity-induced *Arc* transcription was quantified by *Arc* pre-mRNA levels (normalized by *GAPDH* pre-mRNA).

(B–E) Neurons were incubated with BD98 for 20 min and co-treated with triptolide and Bic + 4AP as indicated. ChIP assays were performed with antibodies against SPT6, Rpb1-NTD, and Rpb1-pS2. Levels of SPT6 in the *Arc* gene body are displayed in (B). Total RNA Pol II levels at the *Arc* promoter are displayed in (C). Total RNA Pol II levels in the gene body, normalized to total RNA Pol II at the promoter, are shown in (D). Rpb1-pS2 levels in the gene body, normalized to total RNA Pol II at the promoter, are displayed in (E).

(F–H) In a parallel set of experiments, neurons were treated as in (B)–(E), except they were incubated with BRM014 prior to experiencing activity. Total RNA Pol II levels at the

Arc promoter are displayed in (F). Total RNA Pol II levels in the gene body, normalized to total RNA Pol II at the promoter, are shown in (G). Rpb1-pS2 levels in the gene body, normalized to total RNA Pol II at the promoter, are displayed in (H). Gray dots represent biological replicates; error bars show SE of the mean. *$p < 0.05$, **$p < 0.01$, and **$p < 0.001$. One-way ANOVA statistical analyses were performed followed by Tukey's *post hoc* test.

KEY RESOURCES TABLE

REAGENT OR RESOURCE	SOURCE	IDENTIFIER
Antibodies		
Phospho-Rpb1 CTD (Ser2) (EZ3G)	Cell Signaling Technology	Cat#: 13499 Rabbit mAb RRID: AB_2798238
Rpb1 NTD (D8L4Y)	Cell Signaling Technology	Cat#: 14958s Rabbit mAb RRID: AB_2687876
SMARCC2/BAF170 (D8O9V)	Cell Signaling Technology	Cat #:12760 Rabbit mAb RRID: AB_2798017
Phospho-Rpb1 CTD (Ser5) (D9N5I)	Cell Signaling Technology	Cat #: 13523S Rabbit mAb RRID: AB_2798246
SPT6 (D6J9H)	Cell Signaling Technology	Cat#: 15616S Rabbit mAb RRID: AB_2798748
Brg-1 (G-7)	Santa Cruz Biotechnology, Inc.	Cat #: sc-17796 Mouse RRID: AB_626762
ARID1B/BAF250B (E9J4T)	Cell Signaling Technology	Cat #: 92964 Rabbit mAb RRID: AB_2800195
BAF53b (ACTL6B)	Neuromab Antibodies Inc.	Cat #: 75-311 NeuroMab clone N332B/15 RRID: AB_2315811
CDK9 (D-7)	Santa Cruz Biotechnology	Cat#: sc-13130 Mouse mAb RRID: AB_627245
CDK9 (C12F7)	Cell Signaling Technology	Cat#: 2316 Rabbit mAb RRID: AB_2291505
Histone H2B (53H3)	Cell Signaling Technology	Cat: 2934S Mouse mAb RRID: AB_2295301
Histone H3 (1B1B2)	Cell Signaling Technology	Cat #: 14269 Mouse mAb RRID: AB_2148405
ARID1A/BAF250A (D2A8U)	Cell Signaling Technology	Cat#: 12354 Rabbit mAb RRID: AB_2637010
DPFI	DSHB	Cat: PCRP-DPF1-1A9 RRID: AB_2618559
SS18L1	Santa Cruz Biotechnology, Inc.	Cat: sc-50914; Ms mAb RRID: AB_2195160
ARID1A/BAF250A (PSG3)	Santa Cruz Biotechnology, Inc.	Cat# sc-32761; Ms mAb RRID: AB_673396
Goat anti-Rabbit IgG (H+L) Highly Cross-Adsorbed Secondary Antibody, Alexa Fluor™ 488	Life Technologies	Catalog # A-11034 RRID: A11034
Goat anti-Mouse IgG (H+L) Highly Cross-Adsorbed Secondary Antibody, Alexa Fluor™ 647	Life Technologies	Catalog # A-21236 RRID: A21236
Chemicals, peptides, and recombinant proteins		
ACBI1	OpnMe, Boehringer Ingelheim International	N/A
BRM014, ATP Inhibitor-1	MedChemExpress	Cat# HY-119374
FHT-1015 SMARCA4/SMARCA2 ATPase	MedChemExpress	Cat# HY-144896
BD98 (BRD-K98645985)	MedChemExpress	Cat# HY-114268
BRD7i 2–77	OpnMe, Boehringer Ingelheim International	N/A
BRD9i	Cayman Chemical	Cat# 17749
VZ-185	OpnMe, Boehringer Ingelheim International	N/A
MC180295	MedChemExpress	Cat# HY-119940

REAGENT OR RESOURCE	SOURCE	IDENTIFIER
Flavopiridol	Selleck Chemicals	Cat# S1230
THAL-SNS-032	MedChemExpress	Cat# HY-123937
Critical commercial assays		
Thermo Scientific™ GeneJET Plasmid Maxiprep Kit	Fisher Scientific	Cat# FERK0492
Thermo Scientific™ Pierce™ 16% Formaldehyde (w/v), Methanol-free	Fisher Scientific	Cat # 28906
Thermo Scientific™ Pierce™ Protein A/G Magnetic Beads	Fisher Scientific	Cat # PI88803
One Step RT-PCR BUFFER 5X	QIAGEN	Cat# 1060158
dNTP Mix	QIAGEN	Cat#: 1060159
PerfeCTa® SYBR® Green FastMix® (1250 reactions)	VWR	Catalog # 101414-270
RNASPIN MINI (250)	Cytiva	Cat # 25050072
Protease/Phosphatase Inhibitor Cocktail (100X)	Cell Signaling Technology	Cat # 5872S
4× Laemmli sample buffer	Bio-Rad	Cat# 1610747
10% β-mercaptoethanol	Sigma	Cat# 63689
4–20% gels	Bio-Rad	Cat# 456-8095
4–15% gels	Bio-Rad	Cat# 456-1083
HBSS plus Ca2+and Mg2+	Gibco	Cat# 14025092
HBSS lacking Ca2+and Mg2+	Gibco	Cat# 14175095
StemPro ® Accutase	Life Technologies	Cat# A1110501
Neurobasal medium	Gibco	Cat# 21103049
Monosodium Glutamate	Sigma- Aldrich	Cat# 1446600
L-glutamine	Sigma-Aldrich	Cat# G8540
(+)- Bicuculline	Sigma-Aldrich	Cat# 14340
4-aminopyridine	Acros Organics	Cat# 104571000
Deposited data		
Mass Spectrometry raw data files	jPOST database	JPST003157
Mass Spectrometry raw data files	ProteomeXchange	PXD052840
Experimental models: Organisms/strains		
Sprague-Dawley rats	Charles River	Time pregnant
Oligonucleotides		
GAPDH Forward Intro-exon based AACATGCACAGGGTACTTCGAGGA	Saha *et. al.* 2011[51]	N/A
GAPDH Reverse Intro-exon based ACGACATACTCAGCACCAGCATCA	Saha *et. al.* 2011[51]	N/A
Arc Forward Distance from TSS: +200 bp GAATTTGCTATGCCAACTCACGGG	Saha *et. al.* 2011[51]	N/A
Arc Reverse Distance from TSS: +200 bp AGTCATGGAGCCGAAGTCTGC TTT	Saha *et. al.* 2011[51]	N/A
Gadd45g Forward Distance from TSS: +91 bp CGCGGATCGTCTT TGGGAATCTTT	Saha *et. al.* 2011[51]	N/A
Gadd45g Reverse Distance from TSS: +91bp CATTGTGCGATCC ACGAACAGCAA	Saha *et. al.* 2011[51]	N/A
Cyr61 Forward Distance from TSS: +17 bp TAGAGAAGCGCCTGCAATC	Saha *et. al.* 2011[51]	N/A

REAGENT OR RESOURCE	SOURCE	IDENTIFIER
Cyr61 Reverse Distance from TSS: +17 bp GGAGTGCGGTGAGATGAG	Saha *et. al.* 2011[51]	N/A
Btg2 Forward Intro-exon based CTCTCTCTCTTGTTTCCTCCACAG	Saha *et. al.* 2011[51]	N/A
Btg2 Reverse Intro-exon based TGTGGTTGATGCGGATACAGCGAT	Saha *et. al.* 2011[51]	N/A
Dusp 1 Forward Intro-exon based CTCTACGACCAGGTTAGTAGGAGT	Saha *et. al.* 2011[51]	N/A
Dusp 1 Reverse Intro-exon based ACAGCCGCTTTCTCTATTCTCCCT	Saha *et. al.* 2011[51]	N/A
Nr4a3 Forward Intro-exon based ATGGAGTGTCAACTGGCTTCTGAG	Saha *et. al.* 2011[51]	N/A
Nr4a3 Reverse Intro-exon based GCCATAAGTCTGCGTGGCATAAGT	Saha *et. al.* 2011[51]	N/A
Zif268 Forward Intro-exon based TTCGGCTCTCATCGTCCAGTGATT	Saha *et. al.* 2011[51]	N/A
Zif268 Reverse Intro-exon based AACCGGGTAGTTTGGCTGGGATAA	Saha *et. al.* 2011[51]	N/A
Ppp1r15a Forward Intro-exon based ACAATGACTCAGTGCTGTGACCTG	Saha *et. al.* 2011[51]	N/A
Ppp1r15a Reverse Intro-exon based AGAAAGAGTGGGCTTCCTTCCAGT	Saha *et. al.* 2011[51]	N/A
Gadd45g Forward Intro-exon based ACTCACGGCGCTTGTTCTTTCACA	Saha *et. al.* 2011[51]	N/A
Gadd45g Reverse Intro-exon based ATTCAGGACTTTGGCGGACTCGTA	Saha *et. al.* 2011[51]	N/A
Arc Forward Distance from TSS: +56 bp TTTAGTGCAGTGCTCTGGCGAGTAGT	Saha *et. al.* 2011[51]	N/A
Arc Reverse Distance from TSS: +56 bp TCAAGCTGAAGAGGCCCAGAGA	Saha *et. al.* 2011[51]	N/A
cFos Forward Distance from TSS: + 20 bp GCAACTGAGAAGACT GGATAGA	Saha *et. al.* 2011[51]	N/A
cFos Reverse Distance from TSS: + 20 bp GGGTAGACACTGGTGGGA	Saha *et. al.* 2011[51]	N/A
Btg2 Forward Distance from TSS: +99bp CTCCCCGAGTGGTATGAAAG	Saha *et. al.* 2011[51]	N/A
Btg2 Reverse Distance from TSS: +99 bp TCAAGGTTTTCAGTAGGGCG	Saha *et. al.* 2011[51]	N/A
Dusp 1 Forward Distance from TSS: +300bp TTGGACGTGTTGGAAGAGTTTGGC	Saha *et. al.* 2011[51]	N/A
Dusp 1 Reverse Distance from TSS: +300 bp TGGCTCCAGTGATCAGAGATAGGA	Saha *et. al.* 2011[51]	N/A
Gadd45g Forward Distance from TSS: +91 bp CGCGGATCGTCTTTGGGAATCTTT	Saha *et. al.* 2011[51]	N/A
Gadd45g Reverse Distance from TSS: +91bp CATTGTGCGATCCACGAACAGCAA	Saha *et. al.* 2011[51]	N/A
Cyr61 Forward Distance from TSS: +17 bp TAGAGAAGCGCCTGCAATC	Saha *et. al.* 2011[51]	N/A
Cyr61 Reverse Distance from TSS: +17 bp GGAGTGCGGTGAGATGAG	Saha *et. al.* 2011[51]	N/A
Arc gene body Forward TGTCCCAGATCCAGAACCACATGA	Saha *et. al.* 2011[51]	N/A
Arc gene body Reverse TCTTCACCGAGCCCT GTTTGAACT	Saha *et. al.* 2011[51]	N/A
Software and algorithms		

REAGENT OR RESOURCE	SOURCE	IDENTIFIER
GraphPad Prism version10	Graphpad Software, LLC.	https://www.graphpad.com/scientific-software/prism/
BioRender	BioRender	https://www.biorender.com